Wide-angle photo- and electroproduction of pions to twist-3 accuracy

P. Kroll

Fachbereich Physik, Universität Wuppertal, D-42097 Wuppertal, Germany

K. Passek-Kumerički

Division of Theoretical Physics, Rudjer Bošković Institute, HR-10002 Zagreb, Croatia

We investigate wide-angle photo- and electroproduction of pions within the handbag mechanism in which the $\gamma^{(*)}N \to \pi N'$ amplitudes factorize into hard partonic subprocess amplitudes, $\gamma^{(*)}q \to \pi q'$, and form factors representing $1/x$-moments of generalized parton distributions (GPDs). The subprocess is calculated to twist-3 accuracy taking into account the 2- and 3-body Fock components of the pion. Both components are required for achieving gauge invariance in QED and QCD. The twist-2 and twist-3 distribution amplitudes (DAs) of the pion as well as the form factors are taken from our study of π^0 photoproduction. Extensive results on photoproduction of charged pions are presented and compared to experiment. Predictions on electroproduction of pions as well as on spin effects are also given. As a byproduct of our analysis we also obtain the complete twist-3 subprocess amplitudes contributing to deeply virtual electroproduction of pions.

I. INTRODUCTION

Hard exclusive processes have attracted much attention in recent years. The main interest has been focused on the deeply virtual processes for which the virtuality of the photon provides the hard scale. Examples for such processes are deep-virtual Compton scattering or meson production (DVMP). The basis of the theoretical treatment of these processes is the representation of the amplitudes as a convolution of a hard partonic subprocess and soft hadronic matrix elements, parametrized as generalized parton distributions (GPDs) [1,2]. Besides the deeply virtual processes also wide-angle ones have been investigated for which the hard scale is provided by a large momentum transfer from the photon to the meson. Large momentum transfer is equivalent to large Mandelstam variables s, $-t$ and $-u$. The first process of this type, studied within this handbag mechanism, has been wide-angle Compton scattering (WACS). There are reasonable arguments [3,4] that, for this kinematical situation, the Compton amplitude factorize into a product of perturbatively calculable partonic subprocess amplitudes and form factors of the nucleon representing $1/x$-moments of zero-skewness GPDs. Since the relevant GPDs in this case, H, E and

$\tilde{H}$ at zero-skewness for valence quarks are known from an analysis of the nucleon's electromagnetic form factors [5,6] one can compute the Compton form factors and subsequently the Compton cross section. The results agree fairly well with experiment [7]. We stress that in this calculation no free parameter is fitted to the WACS data. The authors of Ref. [8] extended the approach advocated for in [4] to photoproduction of uncharged pions and ρ mesons. It however turned out that the calculated cross sections are way below the experimental data. An attempt [9] to improve this (twist-2) analysis by taking into account twist-3 contributions in the Wandzura-Wilczek (WW) approximation, i.e., with only the $q\bar{q}$ Fock component of the pion considered, failed too—the twist-3 contribution in WW approximation is zero in wide-angle photoproduction of pions. This is in sharp contrast to DVMP where the WW approximation is nonzero [10,11] and plays an important role in the interpretation of the data on deeply virtual pion electroproduction [12–14]. With the arrival of the CLAS data [15] on wide-angle photoproduction of π^0 mesons the handbag mechanism has again been taken up by us [16]. Now, as a further development of the previous study [9], the full twist-3 contribution to the subprocess amplitude is included in the analysis. Both its parts, the one from the $q\bar{q}$ Fock component of the pion as well as that from its $q\bar{q}g$ Fock component, are connected by the equations of motion and both are required to accomplish gauge invariance. The twist-3 contributions to the hard subprocess go along with leading-twist transversity GPDs, H_T, $\bar{E}_T$ and $\tilde{H}_T$ and the corresponding form factors. We stress that this twist-3

effect, although being formally suppressed by $\mu_\pi/\sqrt{s}$ at the amplitude level, is very strong due to the large mass parameter, μ_π. As shown in [16] the twist-3 contribution dominates the twist-2 one analogously to the case of deeply virtual π^0 electroproduction [11,13,14]. The outcome of [16] is that the CLAS photoproduction data [15] can be fitted with reasonable pion distribution amplitudes (DAs) and soft form factors. Twist-3 effects may also be generated by twist-3 GPDs [17] for which no enhancement similar to μ_π parameter is known. These twist-3 effects are expected to be small and are therefore neglected in [16] as well as in the present work.

The present work is an extension of our previous analysis of wide-angle π^0 photoproduction [16]. We now apply the handbag mechanism to twist-3 accuracy to wide-angle photoproduction of charged pions and, in addition, we also investigate wide-angle electroproduction of pions. The latter process with its large variety of observables may allow for a detailed study of the dynamics of this process and to fix the pion DAs and form factors in detail. The large $-t$ behavior of the transversity form factors encodes the large-t behavior of the transversity GPDs. The latter is required for the understanding of the parton densities in the transverse position plane. We think that the present study is timely because of planned experiments at the Jefferson laboratory.

The paper is organized as follows: In Sec. II we recapitulate the handbag approach to photo- and electro-production of pions to twist-3 accuracy. In the next section, Sec. III, we present the results for the subprocess amplitudes and discuss their properties as well as their photo-production limit, $Q^2 \to 0$, and the DVMP limit, $\hat{t} \to 0$, for which the subprocess amplitudes also hold. The soft physics input to the handbag mechanism, namely the pion DAs and the form factors, are discussed in Sec. IV. In the next section, Sec. V, our results for photoproduction of charged pions are presented and compared to experiment. In Sec. VI we show predictions for the partial cross sections of pion electroproduction. Section VII is devoted to a discussion of spin effects and in Sec. VIII remarks are made concerning the uncertainties of our predictions. The paper ends with the usual summary. In an Appendix we compile the familiar evolution properties of the DAs.

II. THE HANDBAG MECHANISM

The arguments for factorization in the wide-angle region of electroproduction are the same as for Compton scattering [4] and photoproduction [8]. Thus, we can restrict ourselves to the repetition of the most important arguments for factorization and the phenomenological ingredients of the handbag mechanism. Prerequisite for factorization of the electroproduction amplitudes into hard subprocesses and soft form factors, is that the Mandelstam variables s, $-t$ and $-u$ are much larger than Λ^2 where Λ is a typical

hadronic scale of order 1 GeV. The virtuality of the photon, Q^2, is not regarded as a hard scale. Thus,

$$Q^2 < -t, \qquad -u. \tag{1}$$

The mass of the pion is neglected. Corrections due to the nucleon mass, m, of order m^2/s or higher are also neglected. It is advantageous to work in a symmetrical frame which is a center-of-mass frame (c.m.s.) rotated in such a way that the momenta of the ingoing (p) and outgoing (p') nucleons have the same light-cone plus components. In this frame the skewness, defined by

$$\xi = \frac{(p - p')^+}{(p + p')^+}, \tag{2}$$

is zero. Starting from a c.m.s. in which the ingoing proton moves along the 3-direction whereas the outgoing one is scattered by an angle θ in the 1-3 plane, one needs a rotation in that plane by an angle ϑ, defined by the condition

$$|\mathbf{p}|(1 + \cos\vartheta) = |\mathbf{p}'|(1 + \cos(\vartheta - \theta)) + \mathcal{O}(m^2/s), \tag{3}$$

in order to arrive at the symmetric frame ($\mathbf{p}$ and $\mathbf{p}'$ are the 3-momenta of the nucleons). The solution of the condition (3) is

$$\cos\vartheta = \frac{-1}{s + Q^2}\frac{1}{Q^4 - 4st}[Q^2(Q^4 + sQ^2 - 2st) + 4st\sqrt{-us}] + \mathcal{O}(m^2/s). \tag{4}$$

In the photoproduction limit, $Q^2 \to 0$, this becomes

$$\cos\vartheta \to \sqrt{\frac{-u}{s}} = \cos\theta/2 + \mathcal{O}(m^2/s). \tag{5}$$

In the new, rotated, c.m.s. the nucleon momenta read

$$p = \left[p^+, \frac{(s + Q^2)^2}{8sp^+}\sin^2\vartheta, -\frac{s + Q^2}{2\sqrt{s}}\sin\vartheta, 0\right],$$

$$p' = \left[p^+, \frac{s}{8p^+}\sin^2(\vartheta - \theta), -\frac{\sqrt{s}}{2}\sin(\vartheta - \theta), 0\right], \tag{6}$$

where

$$p^+ = -\frac{st}{Q^4 - 4st}(\sqrt{s} + \sqrt{-u} + Q^2/(2\sqrt{s})) + \mathcal{O}(m^2/s). \tag{7}$$

The parametrization of the momenta of the virtual photon, q, and of the meson, q', is obvious. As for wide-angle Compton scattering or photoproduction of mesons it is assumed that the parton virtualities are restricted by $k_i^2 < \Lambda^2$ and that the intrinsic transverse parton momenta, $k_{\perp i}$, defined with

respect to their parent hadron's momentum, satisfy the condition $k_{\perp i}^2/x_i < \Lambda^2$. Here, x_i denotes the momentum fraction that parton i carries. On these premises one can show that the subprocess Mandelstam variables $\hat{s}$ and $\hat{u}$ coincide with those of the full process, meson electroproduction off nucleons, up to corrections of order Λ^2/s,

$$\hat{t} = t, \qquad \hat{s} = (k_j + q)^2 \simeq (p + q)^2 = s,$$
$$\hat{u} = (k_j' - q)^2 \simeq (p' - q)^2 = u, \tag{8}$$

where k_j and $k_j' = k_j + q - q'$ denote the momenta of the active partons, i.e., the partons to which the photon couples. Thus, the active partons are approximately on-shell, move collinear with their parent hadrons and carry a momentum fraction close to unity, $x_j, x_j' \simeq 1$. As in deeply virtual exclusive scattering, the physical situation is that of a hard parton-level subprocess, $\gamma^* q_a \to P q_b$ ($P = \pi^\pm, \pi^0$), and a soft emission and reabsorption of quarks from the nucleon. Up to corrections of order $\Lambda/\sqrt{-t}$ the light-cone helicity amplitudes for wide-angle electroproduction of pions, $\mathcal{M}^P_{0\nu',\mu\nu}$, are then given by a product of subprocess amplitudes, $\mathcal{H}$, which will be discussed in Sec. III, and form factors, R_i and S_i, which parametrize the soft physics that controls the emission from and reabsorption of a quark by the nucleon,[1]

$$\mathcal{M}^P_{0+,\mu+} = \frac{e_0}{2} \sum_\lambda \left[\mathcal{H}^P_{0\lambda,\mu\lambda}(R^P_V(t) + 2\lambda R^P_A(t)) \right.$$
$$\left. - 2\lambda \frac{\sqrt{-t}}{2m} \mathcal{H}^P_{0-\lambda,\mu\lambda} \bar{S}^P_T(t) \right],$$
$$\mathcal{M}^P_{0-,\mu+} = \frac{e_0}{2} \sum_\lambda \left[\frac{\sqrt{-t}}{2m} \mathcal{H}^P_{0\lambda,\mu\lambda} R^P_T(t) \right.$$
$$\left. - 2\lambda \frac{t}{2m^2} \mathcal{H}^P_{0-\lambda,\mu\lambda} S^P_S(t) \right] + e_0 \mathcal{H}^P_{0-,\mu+} S^P_T(t), \tag{9}$$

where μ denotes the helicity of the virtual photon and ν (ν') is the helicity of the ingoing (outgoing) nucleon. The helicity of the active incoming quark is denoted by λ and e_0 is the positron charge. Note that, for the sake of legibility, helicities are labeled by their signs only.

The soft form factors, R^P_i and S^P_i, represent specific flavor combinations of $1/x$-moments of zero-skewness GPDs. The form factors R^P_V, R^P_A and R^P_T are related to the helicity nonflip GPDs H, $\tilde{H}$ and E, respectively. The S-type form factors, S^P_T, $\bar{S}^P_T$ and S^P_S are related to the helicity-flip or transversity GPDs H_T, $\bar{E}_T$ and $\tilde{H}_T$, respectively. The GPDs $\tilde{E}$ and $\tilde{E}_T$ and their associated form factors decouple at zero skewness.

The amplitudes for helicity configurations other than appearing in (9) follow from parity invariance

$$\mathcal{M}^P_{0-\nu',-\mu-\nu} = -(-1)^{\mu-\nu+\nu'} \mathcal{M}^P_{0\nu',\mu\nu}. \tag{10}$$

An analogous relation holds for the subprocess amplitudes $\mathcal{H}$. With the help of (10) the amplitudes for longitudinally polarized photons simplify drastically

$$\mathcal{M}^P_{0+,0+} = e_0 \mathcal{H}^P_{0+,0+} R^P_A(t),$$
$$\mathcal{M}^P_{0-,0+} = e_0 \mathcal{H}^P_{0-,0+} S^P_T(t). \tag{11}$$

In contrast to the transverse amplitudes, twist-2 and twist-3 contributions are separated here: The nucleon helicity nonflip amplitude, $\mathcal{M}^P_{0+,0+}$, is pure twist-2 while the flip one is of twist-3 nature.[2]

The handbag mechanism can be interpreted as Feynman's end-point mechanism [5]. As we said above the handbag mechanism is restricted to the kinematical situation where all three Mandelstam variables are sufficiently large compared to the hadronic scale Λ^2. It is, however, conceivable that in the asymptotic regime of very large Mandelstam variables the hard perturbative mechanism [18,19], for which all partons inside the nucleon participate in the hard process, dominates. Since each additional parton requires one more hard gluon to be exchanged, the higher Fock components of the nucleon are suppressed by inverse powers of s compared to the valence Fock component. This is to be contrasted with the handbag mechanism where there is only one active parton. All other partons inside the nucleon are spectators and the summation goes over all Fock components. Thus, it appears to be plausible that the handbag mechanism provides a larger contribution than the hard perturbative mechanism at least at large but not asymptotically large Mandelstam variables. Indeed the latter mechanism provides results for form factors and WACS which are way below experiment if evaluated from plausible DAs. A calculation of wide-angle photoproduction within that approach has only attempted once [20]. The results are at drastic variance with experiment [21] and need verification since the applied integration method is questionable and is known to fail for WACS [22,23].

III. THE SUBPROCESS AMPLITUDES

The calculation of the amplitudes for the subprocess $\gamma^* q_a \to P q_b$ to twist-3 accuracy is a straightforward generalization of our calculation of the process $\gamma q_a \to \pi^0 q_a$ [16]. In the definitions of the soft pion and nucleon matrix

---

[1] $t_{\min}$ is neglected in the wide-angle region.

[2] In electroproduction of charged pions there is also a contribution from the pion pole. Even though the pole is important in the DVMP region it can be neglected in the wide-angle region where the pole at $t = m_\pi^2$ is very far away.

elements we are using light-cone gauge: the plus component of the gluon field is zero. All possible Wilson lines become unity in that gauge. It is to be stressed that our method for calculating the subprocess amplitudes is similar to the light-cone collinear factorization approach advocated for in [24,25] for the case of electroproduction of transversely polarized vector mesons.

Typical lowest-order Feynman graphs for the process of interest are depicted in Fig. 1. The four graphs of type (a) are relevant for the 2-body contributions. With the help of the projector of a massless $q\bar{q}$ pair on an outgoing massless pion [9,26] ($P = \pi^{\pm}, \pi^0$, isospin invariance is assumed)

$$\mathcal{P}^{P(ab)}_{2,lm} = \frac{f_{\pi}}{2\sqrt{2}N_C} \mathcal{C}^{ab}_P \frac{\delta_{lm}}{\sqrt{N_C}} \left\{ \frac{\gamma_5}{\sqrt{2}} \not{q}' \phi_{\pi}(\tau,\mu_F) + \mu_{\pi}(\mu_F) \frac{\gamma_5}{\sqrt{2}} \right.$$
$$\left. \times \left[\phi_{\pi p}(\tau,\mu_F) - \frac{i}{6}\sigma_{\mu\nu}\frac{q'^{\mu}k'^{\nu}_j}{q' \cdot k'_j}\phi'_{\pi\sigma}(\tau,\mu_F) + \frac{i}{6}\sigma_{\mu\nu}q'^{\mu}\phi_{\pi\sigma}(\tau,\mu_F)\frac{\partial}{\partial k_{\perp\nu}} \right] \right\}_{k_{\perp} \to 0} \quad (12)$$

the subprocess amplitudes for the twist-2 and the 2-body twist-3 contributions can easily be calculated. The familiar twist-2 DA is denoted by ϕ_{π} whereas $\phi_{\pi p}$ and $\phi_{\pi\sigma}$ are the two 2-body twist-3 DAs. The DA $\phi'_{\pi\sigma}$ is the derivative of $\phi_{\pi\sigma}$ with respect to the momentum fraction, τ, the quark entering the meson carries. Their definitions can be found for instance in Appendix A of [16]. For convenience we omit their scale dependence (see the Appendix) in the list of variables in the following. Furthermore, f_{π} in (12) is the usual decay constant of the pion ($f_{\pi} = 132$ MeV); $a(l)$ and

$b(m)$ represent flavor (color) labels of the quark and antiquark, respectively. N_C is the number of colors. The Dirac labels are omitted for convenience. The flavor weight factors are

$$\mathcal{C}^{uu}_{\pi^0} = -\mathcal{C}^{dd}_{\pi^0} = \frac{1}{\sqrt{2}}, \qquad \mathcal{C}^{ud}_{\pi^+} = \mathcal{C}^{du}_{\pi^-} = 1. \quad (13)$$

All other $\mathcal{C}^{ab}_P$ are zero.

In (12), $k_{\perp}$ denotes the intrinsic transverse momentum of the quark entering the meson. It is defined with respect to the meson's momentum, q'. The quark and antiquark momenta are thus given by

$$k_q = \tau q' + k_{\perp}, \qquad k_{\bar{q}} = \bar{\tau}q' - k_{\perp}, \quad (14)$$

where $\bar{\tau} = 1 - \tau$ and $q' \cdot k_{\perp} = 0$. After the derivative in (12) is performed the collinear limit, $k_{\perp} = 0$, is to be taken.

The mass parameter μ_{π} is large since it is the pion mass, m_{π}, enhanced by the chiral condensate

$$\mu_{\pi} = \frac{m^2_{\pi}}{m_u + m_d}, \quad (15)$$

by means of the divergence of the axial-vector current. Here, $m_{u(d)}$ are the current-quark masses of the pion's constituents. Following [10,11] we take the value 2 GeV for this parameter at the initial scale $\mu_0 = 2$ GeV. Its uncertainty is, however, large.[3] The mass parameter evolves with the scale; see the Appendix. For the factorization and renormalization scale we choose

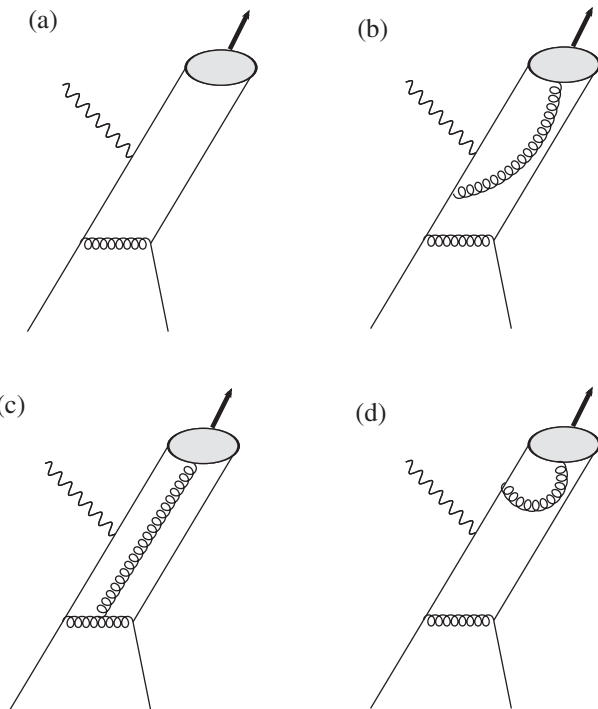$$\mu^2_R = \mu^2_F = \frac{\hat{t}\,\hat{u}}{\hat{s}}, \quad (16)$$

FIG. 1. Typical leading-order Feynman graphs for $\gamma^* q \to Pq$. (a) For the 2-body twist-2 and twist-3 Fock components of the meson. (b) and (c) Contributions from the $q\bar{q}g$ Fock component with and without triple gluon coupling. (d) A soft contribution which is to be considered as a part of the 2-body twist-3 DAs.

_____

[3]Using, for instance, the values for the current-quark masses quoted in [27], one obtains $\mu_{\pi}(\mu_0) = 2.64^{+0.11}_{-0.42}$ GeV for the case of the π^0. Values of 1.8 GeV and 1.9 GeV at μ_0 are advocated for in [28,29], respectively.

which takes care of the requirement that both t and u should be large. The strong coupling, $\alpha_s(\mu_R)$, is evaluated in the one-loop approximation from $\Lambda_{\text{QCD}} = 0.22$ GeV and four flavors ($n_f = 4$).

A. The twist-2 subprocess amplitudes

As shown in [8] at leading-order (LO) of perturbative QCD the twist-2 (light-cone) helicity amplitude for transversely polarized photons reads

$$
\begin{aligned}
\mathcal{H}_{0\lambda,\mu\lambda}^{P,tw2} = &\frac{1}{2}\kappa_P^{(ab)}f_\pi\frac{\sqrt{-\hat{t}}}{\hat{s}+Q^2}\int_0^1 d\tau\phi_\pi(\tau) \\
&\times\Bigg[(1+2\lambda\mu)\Bigg(\frac{(\hat{s}\tau+Q^2)(\hat{s}+Q^2)-\hat{u}Q^2\bar{\tau}}{\hat{s}\,\bar{\tau}(Q^2\bar{\tau}-\hat{t}\tau)}e_a \\
&+\frac{(\hat{s}\tau-Q^2)(\hat{s}+Q^2)-\hat{u}Q^2\bar{\tau}}{\hat{u}\tau(Q^2\tau-\hat{t}\,\bar{\tau})}e_b\Bigg) \\
&-(1-2\lambda\mu)\Bigg(\frac{\hat{u}e_a}{(Q^2\bar{\tau}-\hat{t}\tau)}+\frac{\hat{s}\,\bar{\tau}\,e_b}{\tau(Q^2\tau-\hat{t}\,\bar{\tau})}\Bigg)\Bigg],
\end{aligned}
\tag{17}
$$

and for longitudinally polarized photons

$$
\begin{aligned}
\mathcal{H}_{0\lambda,0\lambda}^{P,tw2} = &2\sqrt{2}\lambda\kappa_P^{(ab)}f_\pi\frac{Q\sqrt{-\hat{u}\,\hat{s}}}{\hat{s}+Q^2}\int_0^1 d\tau\phi_\pi(\tau) \\
&\times\Bigg(\frac{\hat{u}e_a}{\hat{s}(Q^2\bar{\tau}-\hat{t}\tau)}-\frac{(\hat{t}+\tau\hat{u})e_b}{\tau\hat{u}(Q^2\tau-\hat{t}\,\bar{\tau})}\Bigg),
\end{aligned}
\tag{18}
$$

where

$$
\kappa_P^{(ab)} = 2\sqrt{2}\pi\alpha_s(\mu_R^2)\mathcal{C}_P^{ab}\frac{C_F}{N_C}.
\tag{19}
$$

As usual, $C_F = (N_C^2-1)/(2N_C)$ is a color factor and $e_a(e_b)$ is the charge of the flavor-$a(b)$ quark in units of the positron charge. The summation over the same flavor labels is understood. The twist-2 contribution only affects the subprocess amplitudes for quark helicity nonflip, the quark helicity-flip amplitudes are zero. Leaving aside the pion DA the subprocess amplitudes are expressed in terms of the Lorentz invariant Mandelstam variables. Thus, in any other c.m.s. the expressions (17) and (18) hold too. In any case we assume that in the symmetric frame the pion DA is the usual one.

In the photoproduction limit, $Q^2 \to 0$, the longitudinal amplitude vanishes $\propto Q$ (see Table I). For the transverse amplitude, taking into account the $\tau \to \bar{\tau}$ symmetry property of pion DA, we recover the result derived in [8] which we explicitly quote for later use:

$$
\begin{aligned}
\mathcal{H}_{0\lambda,\mu\lambda}^{P,tw2}\xrightarrow{Q^2\to 0}&\frac{1}{2}\kappa_P^{(ab)}f_\pi\frac{1}{\sqrt{-\hat{t}}}\int_0^1\frac{d\tau}{\tau}\phi_\pi(\tau) \\
&\times((1+2\lambda\mu)\hat{s}-(1-2\lambda\mu)\hat{u})\left(\frac{e_a}{\hat{s}}+\frac{e_b}{\hat{u}}\right).
\end{aligned}
\tag{20}
$$

B. The 2-body twist-3 contributions

Let us now turn to the 2-body twist-3 contribution to the subprocess amplitudes. It is tightly connected to the 3-body twist-3 contribution through the equations of motion (EOMs). In fact, for light-cone gauge which we have chosen for the vacuum-pion matrix element (more details on that choice for the twist-3 calculation have been given in [16]), the 2-body twist-3 DAs are related to the 3-body one, $\phi_{3\pi}(\tau_a, \tau_b, \tau_g)$, integrated upon the momentum fraction the constituent gluon carries:

$$
\begin{aligned}
\tau\phi_{\pi p}(\tau)+\frac{\tau}{6}\phi_{\pi\sigma}'(\tau)-\frac{1}{3}\phi_{\pi\sigma}(\tau)&=\phi_{\pi 2}^{\text{EOM}}(\bar{\tau}), \\
\bar{\tau}\phi_{\pi p}(\tau)-\frac{\bar{\tau}}{6}\phi_{\pi\sigma}'(\tau)-\frac{1}{3}\phi_{\pi\sigma}(\tau)&=\phi_{\pi 2}^{\text{EOM}}(\tau),
\end{aligned}
\tag{21}
$$

where

$$
\phi_{\pi 2}^{\text{EOM}}(\tau) = 2\frac{f_{3\pi}}{f_\pi\mu_\pi}\int_0^{\bar{\tau}}\frac{d\tau_g}{\tau_g}\phi_{3\pi}(\tau,\bar{\tau}-\tau_g,\tau_g).
\tag{22}
$$

As the 2-body DAs $\phi_{3\pi}$ depends on the factorization scale, see the Appendix. We also omit the scale dependence in its list of variables. The parameter $f_{3\pi}$ plays a similar role as the pion decay constant for the twist-2 DA. It also evolves with the factorization scale.

With the help of the relation (21) for the 2-body twist-3 DAs we can express the corresponding helicity amplitudes in terms of, say, $\phi_{\pi p}$ and $\phi_{\pi 2}^{\text{EOM}}$:

$$
\mathcal{H}^{P,tw3,q\bar{q}} = \mathcal{H}^{P,\phi_{\pi p}}+\mathcal{H}^{P,\phi_{\pi 2}^{\text{EOM}}}.
\tag{23}
$$

Here the $\tau \to \bar{\tau}$ symmetry property of $\phi_{\pi p}$ and $\phi_{\pi\sigma}$ was used. Note that the 3-body DA possesses the symmetry property

$$
\phi_{3\pi}(\tau_a,\tau_b,\tau_g) = \phi_{3\pi}(\tau_b,\tau_a,\tau_g),
\tag{24}
$$

which we also use in the following in order to simplify the expressions for the subprocess amplitudes. For transversely polarized photons we find

$$\mathcal{H}_{0-\lambda,\mu\lambda}^{P,\phi_{\pi p}} = \kappa_P^{(ab)} f_\pi \mu_\pi \frac{\sqrt{-\hat{u}\,\hat{s}}}{\hat{s}+Q^2} \frac{Q^2}{\hat{t}+Q^2} \int_0^1 d\tau \frac{\phi_{\pi p}(\tau)}{Q^2\bar{\tau}-\hat{t}\tau} \times \left\{ \frac{Q^2\hat{u}(2\lambda+\mu) - \hat{s}\,\hat{t}\,(2\lambda-\mu)}{\hat{s}} \right.$$
$$\left. \times \left[\left(\frac{\hat{t}}{Q^2\bar{\tau}-\hat{t}\tau} - 1 \right) \left(\frac{e_a}{\hat{s}} - \frac{e_b}{\hat{u}} \right) + (\hat{t}+Q^2)\frac{e_b}{\hat{u}^2} \right] + 4\mu\hat{t} \left(\frac{e_a}{\hat{s}} - \frac{e_b}{\hat{u}} \right) \right\}, \tag{25}$$

and

$$\mathcal{H}_{0-\lambda,\mu\lambda}^{P,\phi_{\pi2}^{\rm EOM}} = \frac{1}{2}\kappa_P^{(ab)} f_\pi \mu_\pi \frac{\sqrt{-\hat{u}\,\hat{s}}}{\hat{s}+Q^2} \frac{\hat{t}}{\hat{t}+Q^2} \int_0^1 d\tau \phi_{\pi2}^{\rm EOM}(\tau) \left\{ \frac{Q^2\hat{u}(2\lambda+\mu) - \hat{s}\,\hat{t}\,(2\lambda-\mu)}{\hat{s}} \right.$$
$$\times \left[-\left(\frac{Q^2+(Q^2\bar{\tau}-\hat{t}\tau)}{\bar{\tau}(Q^2\bar{\tau}-\hat{t}\tau)^2} + \frac{\hat{t}-(Q^2\tau-\hat{t}\,\bar{\tau})}{\tau(Q^2\tau-\hat{t}\,\bar{\tau})^2} \right) \left(\frac{e_a}{\hat{s}} - \frac{e_b}{\hat{u}} \right) - \left(\frac{\tau}{\bar{\tau}^2(Q^2\bar{\tau}-\hat{t}\tau)} + \frac{1}{\tau(Q^2\tau-\hat{t}\,\bar{\tau})} \right) \frac{\hat{t}+Q^2}{\hat{u}}\frac{e_b}{\hat{u}} \right]$$
$$\left. -2\mu \left(\frac{2Q^2}{\bar{\tau}(Q^2\bar{\tau}-\hat{t}\tau)} + \frac{\hat{t}-Q^2}{\tau(Q^2\tau-\hat{t}\,\bar{\tau})} \right) \left(\frac{e_a}{\hat{s}} - \frac{e_b}{\hat{u}} \right) \right\}. \tag{26}$$

For longitudinally polarized photons we obtain

$$\mathcal{H}_{0-\lambda,0\lambda}^{P,\phi_{\pi p}} = -2\sqrt{2}\kappa_P^{(ab)} f_\pi \mu_\pi(\mu_F^2) \frac{Q\sqrt{-\hat{t}}}{\hat{s}+Q^2} \int_0^1 d\tau \frac{\phi_{\pi p}(\tau)}{Q^2\bar{\tau}-\hat{t}\tau} \left(\frac{\hat{t}(Q^2+\hat{s}\tau)}{Q^2\bar{\tau}-\hat{t}\tau} \left(\frac{e_a}{\hat{s}} - \frac{e_b}{\hat{u}} \right) - Q^2\frac{e_b}{\hat{u}} \right), \tag{27}$$

and

$$\mathcal{H}_{0-\lambda,0\lambda}^{P,\phi_{\pi2}^{\rm EOM}} = -\sqrt{2}\kappa_P^{(ab)} f_\pi \mu_\pi \frac{Q\sqrt{-\hat{t}}}{\hat{s}+Q^2} \int_0^1 d\tau \phi_{\pi2}^{\rm EOM}(\tau) \left[\left(\frac{Q^2\hat{u}}{(Q^2\bar{\tau}-\hat{t}\tau)^2} + \frac{\hat{t}\,\hat{u}}{(Q^2\tau-\hat{t}\,\bar{\tau})^2} \right. \right.$$
$$\left. \left. - \frac{\hat{t}}{\bar{\tau}(Q^2\bar{\tau}-\hat{t}\tau)} + \frac{2Q^2\hat{t}-Q^2\hat{u}+\hat{s}\,\hat{t}}{2\tau Q^2(Q^2\tau-\hat{t}\,\bar{\tau})} \right) \left(\frac{e_a}{\hat{s}} - \frac{e_b}{\hat{u}} \right) + \left(\frac{\hat{t}\tau}{\bar{\tau}^2(Q^2\bar{\tau}-\hat{t}\tau)} + \frac{\hat{t}}{\tau(Q^2\tau-\hat{t}\,\bar{\tau})} \right) \frac{e_b}{\hat{u}} \right]. \tag{28}$$

Because of the derivative with respect to the quark transverse momentum involved in the projector (12) terms proportional to the square of propagators are generated in the amplitudes (25)–(28). All these terms are unproblematic with one exception[4]: the term $\propto Q^2\hat{t}/(\bar{\tau}Q^2 - \tau\hat{t})^2$ in (25) leads to

$$\lim_{Q^2\to0} \mathcal{H}_{0-\lambda,\mu\lambda}^{P,\phi_{\pi p}}(Q^2) = (2\lambda-\mu)\kappa_P^{(ab)} f_\pi \mu_\pi \sqrt{-\frac{\hat{u}}{\hat{s}}} \left(\frac{e_a}{\hat{s}} - \frac{e_b}{\hat{u}} \right) \phi_{\pi p}(0) \tag{29}$$

in the photoproduction limit, $Q^2 \to 0$, provided the integration is performed before the limit is taken. Since the DA $\phi_{\pi p}$ does not vanish at $\tau = 0$ the integral (29) is in conflict with our study of wide-angle pion photoproduction [16] where we found that the $\phi_{\pi p}$ contribution to the subprocess amplitudes is zero. This latter result also implies that the WW approximation is zero in wide-angle photoproduction. We regard this apparent contradiction between photoproduction and the $Q^2 \to 0$ limit of electroproduction as a relic of the $k_\perp$-dependence of the projector (12). Although the term (29) is of minor numerical importance we prefer to have a smooth transition from electro- to photoproduction which we achieve by allowing for a mean-square quark transverse momentum, $\langle k_\perp^2 \rangle$, in the propagator $\bar{\tau}Q^2 - \tau\hat{t}$ of the relevant term

$$\int_0^1 d\tau \phi_{\pi p}(\tau) \frac{Q^2\hat{t}}{(Q^2\bar{\tau}-\hat{t}\tau)^2} \to \int_0^1 d\tau \phi_{\pi p}(\tau) \frac{Q^2\hat{t}}{(Q^2\bar{\tau}-\hat{t}\tau+\langle k_\perp^2 \rangle)^2}. \tag{30}$$

With this regulator, being reminiscent to the $k_\perp$ dependence of the propagator, we arrive at

$$\lim_{Q^2\to0} \mathcal{H}_{0-\lambda,\mu\lambda}^{P,\phi_{\pi p},reg}(Q^2) = 0 \tag{31}$$

---

[4]In this context it is important to realize that $\Phi_{\pi2}^{\rm EOM}$ vanishes at the end points $\tau = 0$ and 1; see Eq. (59) below.

TABLE I. Power behavior of various twist-2 and twist-3 contributions for transverse and longitudinal photons for $Q^2 \to 0$. The singularities (32) and (42) are already subtracted. Note that, according to the prerequisite of the handbag mechanism, $-\hat{t}$ and $-\hat{u}$ are of the order of $\hat{s}$.

$\mathcal{H}$	Transverse	Longitudinal
Twist-2	$\sim \frac{f_\pi}{\sqrt{\hat{s}}}$	$\sim \frac{f_\pi}{\sqrt{\hat{s}}} \frac{Q}{\sqrt{\hat{s}}}$
Twist-3, 2-body, $\phi_{\pi p}$	$\sim \frac{f_\pi \mu_\pi}{\hat{s}} \frac{Q^2}{\hat{s}}$	$\sim \frac{f_\pi \mu_\pi}{\hat{s}} \frac{Q}{\sqrt{\hat{s}}}$
Twist-3, C_F, $\phi_{3\pi}$	$\sim \frac{f_{3\pi}}{\hat{s}}$	$\sim \frac{f_{3\pi}}{\hat{s}} \frac{Q}{\sqrt{\hat{s}}}$
Twist-3, 3-body, C_G	$\sim \frac{f_{3\pi}}{\hat{s}}$	$\sim \frac{f_{3\pi}}{\hat{s}} \frac{Q}{\sqrt{\hat{s}}}$

and so obtain consistency with the photoproduction analysis. Following [10] we adopt the value 0.5 GeV² for $\langle k_\perp^2 \rangle$ in our numerical studies. It is straightforward to show that the subprocess amplitude $\mathcal{H}_{0-\lambda,0\lambda}^{P,\phi_{\pi p}}$, Eq. (27), vanishes in the photoproduction limit $Q^2 \to 0$.

In Table I we list the power behavior of various contributions to the subprocess amplitudes for $Q^2 \to 0$. The $\phi_{\pi 2}^{\text{EOM}}$ part for longitudinally polarized photons, Eq. (28), is singular in the photoproduction limit

$$\mathcal{H}_{0-\lambda,0\lambda}^{P,\phi_{\pi 2}^{\text{EOM}}} \xrightarrow{Q^2 \to 0} \frac{1}{\sqrt{2}} \kappa_P^{(ab)} f_\pi \mu_\pi \frac{\sqrt{-\hat{t}}}{Q} \int_0^1 \frac{d\tau}{\tau\bar{\tau}} \phi_{\pi 2}^{\text{EOM}}(\tau) \left(\frac{e_a}{\hat{s}} - \frac{e_b}{\hat{u}} \right).$$

(32)

As we will see in the following section, this singularity is canceled in the full subprocess amplitude by a corresponding singularity in the 3-body contribution. Subtracting the singularity (32) the remaining contribution to $\mathcal{H}_{0-\lambda,0\lambda}^{P,\phi_{\pi 2}^{\text{EOM}}}$ vanishes in the photoproduction limit; see Table I. Hence, the only 2-body twist-3 contribution that survives in the photoproduction limit is $\mathcal{H}_{0-\lambda,\mu\lambda}^{P,\phi_2^{\text{EOM}}}$ as we found in [16].

C. The 3-body twist-3 contributions

Typical lowest order Feynman graphs relevant for the 3-body twist-3 contributions are shown in Fig. 1(b)–1(c). The 16 Feynman graphs (b) and (c) make up the 3-body contribution. Graphs of type (d) for which the constituent gluon of the pion couples to one of its quark constituents, are soft contributions and are to be considered as parts of the 2-body twist-3 meson DA. In light-cone gauge the gluon field, $A_\mu(x)$, appearing in perturbation theory, is related to the gluon field strength tensor $G_{\mu\nu}$ which defines the 3-body DA, $\phi_{3\pi}$, [30] by (n being a lightlike vector)

$$A_\rho^r(z) = \lim_{\epsilon \to 0} n^\nu \int_0^\infty d\sigma e^{-\epsilon\sigma} G_{\rho\nu}^r(z + n\sigma).$$

(33)

In connection with the definition of the 3-body twist-3 DA (see, for instance, [29,31]) this relation between A_μ and $G_{\mu\nu}$ allows to derive the 3-body projector, $q\bar{q}g \to \pi$, to be used in perturbative calculations involving the $q\bar{q}g$ Fock component [16]. For an outgoing pion this projector reads

$$\mathcal{P}_{3,lm}^{P(ab)\rho,r} = \frac{-i}{g} \frac{f_{3\pi}(\mu_F)}{2\sqrt{2N_C}} \mathcal{C}_P^{ab} \frac{(t^r)_{lm}}{C_F\sqrt{N_C}} \frac{\gamma_5}{\sqrt{2}} \sigma_{\mu\nu} q'^\mu g_\perp^{\nu\rho} \frac{\phi_{3\pi}(\tau_a, \tau_b, \tau_g, \mu_F)}{\tau_g}.$$

(34)

The transverse metric tensor is defined as

$$g_\perp^{\nu\rho} = \left(g^{\nu\rho} - \frac{k_j'^\nu q'^\rho + q'^\nu k_j'^\rho}{k_j' \cdot q'} \right),$$

(35)

and $t^r = \lambda^r/2$ is the SU(3) color matrix for a gluon of color r while g denotes the QCD coupling.

For the sake of legibility we split the 3-body contribution into two parts:

$$\mathcal{H}^{P,tw3,q\bar{q}g} = \mathcal{H}^{P,q\bar{q}g,C_G} + \mathcal{H}^{P,q\bar{q}g,C_F}.$$

(36)

The first part is proportional to the color factor

$$C_G = C_F - \frac{1}{2} C_A,$$

(37)

which appears only in the 3-body twist-3 contributions. Here, as usual, $C_A = N_C$. The second part, $\mathcal{H}^{tw3,q\bar{q}g,C_F}$, is proportional to C_F as is the case for the 2-body contributions. For transversely polarized photons the 3-body twist-3 contributions read

$$\mathcal{H}_{0-\lambda,\mu\lambda}^{P,q\bar{q}g,C_G} = \kappa_P^{(ab)} f_{3\pi} \frac{C_G}{C_F} \frac{\sqrt{-\hat{u}\,\hat{s}}}{\hat{s}+Q^2} (Q^2\hat{u}(2\lambda+\mu) - \hat{s}\,\hat{t}\,(2\lambda-\mu)) \left(\frac{e_a}{\hat{s}^2\hat{u}} + \frac{e_b}{\hat{s}\hat{u}^2} \right)$$
$$\times \int_0^1 \frac{d\tau}{\bar{\tau}} \int_0^{\bar{\tau}} \frac{d\tau_g}{\tau_g} \phi_{3\pi}(\tau,\bar{\tau}-\tau_g,\tau_g) \left(\frac{1}{\bar{\tau}-\tau_g} - \frac{\hat{t}}{(Q^2\bar{\tau}-\hat{t}\tau)\tau_g} \right), \tag{38}$$

and

$$\mathcal{H}_{0-\lambda,\mu\lambda}^{P,q\bar{q}g,C_F} = \kappa_P^{(ab)} f_{3\pi} \frac{\sqrt{-\hat{u}\,\hat{s}}}{\hat{s}+Q^2} \int_0^1 d\tau \int_0^{\bar{\tau}} \frac{d\tau_g}{\tau_g} \phi_{3\pi}(\tau,\bar{\tau}-\tau_g,\tau_g) \left\{ \frac{Q^2\hat{u}(2\lambda+\mu) - \hat{s}\,\hat{t}\,(2\lambda-\mu)}{\hat{s}} \right.$$
$$\times \left[\left(\frac{e_a}{\hat{s}} - \frac{e_b}{\hat{u}} \right) \left(\frac{\tau_g}{\bar{\tau}(Q^2\bar{\tau}-\hat{t}\tau)(\bar{\tau}-\tau_g)} + \frac{\hat{t}}{\tau(Q^2\tau-\hat{t}\,\bar{\tau})(Q^2(\tau+\tau_g)-\hat{t}(\bar{\tau}-\tau_g))} \right) \right.$$
$$\left. - \frac{Q^2\tau_g - \hat{t}(1-\tau_g)}{\bar{\tau}(Q^2\bar{\tau}-\hat{t}\tau)(\bar{\tau}-\tau_g)} \frac{e_b}{\hat{u}^2} \right] + \frac{1}{\tau} \frac{2\mu\hat{t}}{Q^2\tau-\hat{t}\,\bar{\tau}} \left(\frac{e_a}{\hat{s}} - \frac{e_b}{\hat{u}} \right) \right\}, \tag{39}$$

respectively. For longitudinally polarized photons they are given by

$$\mathcal{H}_{0-\lambda,0\lambda}^{P,q\bar{q}g,C_G} = 2\sqrt{2}\kappa_P^{(ab)} f_{3\pi} \frac{C_G}{C_F} \frac{Q\sqrt{-\hat{t}}}{\hat{s}+Q^2} \left(\frac{e_a}{\hat{s}} + \frac{e_b}{\hat{u}} \right) \int_0^1 \frac{d\tau}{\bar{\tau}} \int_0^{\bar{\tau}} \frac{d\tau_g}{\tau_g} \phi_{3\pi}(\tau,\bar{\tau}-\tau_g,\tau_g) \left(\frac{1}{\bar{\tau}-\tau_g} - \frac{\hat{t}}{(Q^2\bar{\tau}-\hat{t}\tau)\tau_g} \right), \tag{40}$$

and

$$\mathcal{H}_{0-\lambda,0\lambda}^{P,q\bar{q}g,C_F} = 2\sqrt{2}\kappa_P^{(ab)} f_{3\pi} \frac{Q\sqrt{-\hat{t}}}{\hat{s}+Q^2} \int_0^1 d\tau \int_0^{\bar{\tau}} \frac{d\tau_g}{\tau_g} \phi_{3\pi}(\tau,\bar{\tau}-\tau_g,\tau_g) \left\{ \left(\frac{e_a}{\hat{s}} - \frac{e_b}{\hat{u}} \right) \left(\frac{\hat{u}\tau_g}{\bar{\tau}(Q^2\bar{\tau}-\hat{t}\tau)(\bar{\tau}-\tau_g)} \right. \right.$$
$$\left. + \frac{\hat{t}\,\hat{u}}{\tau(Q^2\tau-\hat{t}\,\bar{\tau})(Q^2(\tau+\tau_g)-\hat{t}(\bar{\tau}-\tau_g))} + \frac{Q^2\hat{u}+\hat{s}\,\hat{t}}{2Q^2\tau(Q^2\tau-\hat{t}\,\bar{\tau})} \right) + \frac{\hat{t}-(\hat{t}+Q^2)\tau_g}{\bar{\tau}(Q^2\bar{\tau}-\tau\hat{t})(\bar{\tau}-\tau_g)} \frac{e_b}{\hat{u}} \right\}. \tag{41}$$

Evidently, $\mathcal{H}_{0-\lambda,0\lambda}^{P,q\bar{q}g,C_F}$ is singular in the photoproduction limit

$$\mathcal{H}_{0-\lambda,0\lambda}^{P,q\bar{q}g,C_F} \xrightarrow{Q^2\to 0} -\sqrt{2}\kappa_P^{(ab)} f_{3\pi} \frac{\sqrt{-\hat{t}}}{Q} \left(\frac{e_a}{\hat{s}} - \frac{e_b}{\hat{u}} \right) \int_0^1 \frac{d\tau}{\tau\bar{\tau}} \int_0^{\bar{\tau}} \frac{d\tau_g}{\tau_g} \phi_{3\pi}(\tau,\bar{\tau}-\tau_g,\tau_g). \tag{42}$$

The τ_g-integral in this relation is just $f_\pi \mu_\pi \phi_{\pi2}^{\text{EOM}}/(2f_{3\pi})$; see (22). Using this we notice that the singular part of $\mathcal{H}_{0-\lambda,0\lambda}^{P,q\bar{q}g,C_F}$ exactly cancels that of $\mathcal{H}_{0-\lambda,0\lambda}^{P,\phi_{\pi2}^{\text{EOM}}}$ given in (32). Subtracting this singularity from $\mathcal{H}_{0-\lambda,0\lambda}^{P,q\bar{q}g,C_F}$ this amplitude vanishes proportional to Q in the photoproduction limit as $\mathcal{H}_{0-\lambda,0\lambda}^{P,q\bar{q}g,C_G}$ does; see Table I.

D. Remarks concerning gauge invariance

Probing current conservation of the twist-3 amplitudes we find that the 2-body twist-3 contributions proportional to $\phi_{\pi p}$ as well as the 3-body twist-3 contributions proportional to C_G respect it while the other two don't. Replacing the photon polarization vector by the corresponding momentum in the $\phi_{\pi2}^{\text{EOM}}$ contribution the term

$$\mathcal{H}_{elm}^{P,\phi_{\pi2}^{\text{EOM}}} = \frac{\kappa_P^{(ab)}}{\sqrt{2}} f_\pi \mu_\pi \sqrt{-\hat{t}}(\hat{t}+Q^2) \left(\frac{e_a}{\hat{s}} - \frac{e_b}{\hat{u}} \right) \int_0^1 \frac{d\tau}{\tau(\bar{\tau}\hat{t}-\tau Q^2)} \phi_{\pi2}^{\text{EOM}} \tag{43}$$

is left over. Expressing $\Phi_{\pi2}^{\text{EOM}}$ through the 3-body DA with the help of Eq. (22) one sees that (43) is canceled by a corresponding term from the 3-body twist-3 contributions proportional to C_F. Hence, the sum of $\mathcal{H}^{P,\phi_2^{\text{EOM}}}$ and $\mathcal{H}^{P,q\bar{q}g,C_F}$ respects current conservation.

We also have proven that the 2- and 3-body twist-3 contributions are separately gauge invariant with respect to the choice of the covariant gluon propagator

$$g^{\mu\nu} - \zeta_c \frac{k_g^\mu k_g^\nu}{k_g^2}, \tag{44}$$

where k_g is the momentum of the virtual gluon and ζ_g an arbitrary gauge parameter. We also checked the invariance of the subprocess amplitudes with respect to axial light-cone gauges [32,33]

$$g^{\mu\nu} - \frac{n^\mu k_g^\nu + n^\nu k_g^\mu}{n \cdot k_g}, \tag{45}$$

where n is an arbitrary lightlike vector and $n \cdot k_g \neq 0$. In contrast to the covariant gauges the separate pieces, $\mathcal{H}^{P,\phi_{\pi2}^{\mathrm{EOM}}}$ and $\mathcal{H}^{P,q\bar{q}g,C_F}$, are not invariant with respect to

axial gauges but their sum does not depend on n. Thus, we can conclude that the twist-3 subprocess amplitudes are QCD gauge invariant. The choice of gauge for the external gluon was discussed in [16].

E. The complete twist-3 amplitude

In order to present finally a gauge invariant result we have to add $\mathcal{H}^{P,\phi_{\pi2}^{\mathrm{EOM}}}$ [(26), (28)] and $\mathcal{H}^{P,q\bar{q}g,C_F}$ [(39), (41)]

$$\mathcal{H}^{P,C_F,\phi_{3\pi}} = \mathcal{H}^{P,\phi_2^{\mathrm{EOM}}} + \mathcal{H}^{P,q\bar{q}g,C_F}. \tag{46}$$

Since $\phi_{\pi2}^{\mathrm{EOM}}$ is an integral upon the 3-body DA $\phi_{3\pi}$, see Eq. (22), the sum (46) can solely be expressed through $\phi_{3\pi}$ and simplifications occur.

For transversely polarized photons the sum (46) reads

$$\mathcal{H}_{0-\lambda,\mu\lambda}^{P,C_F,\phi_{3\pi}} = \kappa_P^{(ab)} f_{3\pi} \frac{\sqrt{-\hat{u}\,\hat{s}}}{\hat{s}+Q^2} \int_0^1 d\tau \int_0^{\bar{\tau}} d\tau_g \phi_{3\pi}(\tau, \bar{\tau}-\tau_g, \tau_g) \left\{ \frac{Q^2\hat{u}(2\lambda+\mu) - \hat{s}\,\hat{t}\,(2\lambda-\mu)}{\hat{s}} \left[\left(\frac{e_a}{\hat{s}} - \frac{e_b}{\hat{u}} \right) \right. \right.$$

$$\times \left(\frac{1}{\bar{\tau}(Q^2\bar{\tau}-\hat{t}\tau)(\bar{\tau}-\tau_g)} - \frac{\hat{t}(\hat{t}+Q^2)}{\tau(Q^2\tau-\hat{t}\,\bar{\tau})^2(Q^2(\tau+\tau_g) - \hat{t}(\bar{\tau}-\tau_g))} \right.$$

$$\left. - \frac{Q^4\hat{t}(\hat{t}-Q^2)(\bar{\tau}-\tau)}{(\hat{t}+Q^2)\tau\bar{\tau}(Q^2\bar{\tau}-\hat{t}\tau)^2(Q^2\tau-\hat{t}\,\bar{\tau})^2\tau_g} \right) - \left(\frac{Q^2\hat{t}(\bar{\tau}-\tau)}{\tau\bar{\tau}(Q^2\bar{\tau}-\hat{t}\tau)(Q^2\tau-\hat{t}\,\bar{\tau})\tau_g} + \frac{1}{\bar{\tau}^2(\bar{\tau}-\tau_g)} \right) \frac{e_b}{\hat{u}^2} \right]$$

$$\left. + 2\mu \left(\frac{e_a}{\hat{s}} - \frac{e_b}{\hat{u}} \right) \frac{2Q^4\hat{t}(\bar{\tau}-\tau)}{(\hat{t}+Q^2)\tau\bar{\tau}(Q^2\bar{\tau}-\hat{t}\tau)(Q^2\tau-\hat{t}\,\bar{\tau})\tau_g} \right\}. \tag{47}$$

For longitudinally polarized photons we have

$$\mathcal{H}_{0-\lambda,0\lambda}^{P,C_F,\phi_{3\pi}} = 2\sqrt{2}\kappa_P^{(ab)} f_{3\pi} \frac{Q\sqrt{-\hat{t}}}{\hat{s}+Q^2} \int_0^1 d\tau \int_0^{\bar{\tau}} d\tau_g \phi_{3\pi}(\tau, \bar{\tau}-\tau_g, \tau_g) \left\{ \left(-\frac{Q^2\hat{u}}{(Q^2\bar{\tau}-\hat{t}\tau)^2\tau_g} - \frac{\hat{t}(Q^2\tau-\hat{t}\,\bar{\tau}) - Q^2\hat{u}\tau}{\tau(Q^2\tau-\hat{t}\,\bar{\tau})^2\tau_g} \right. \right.$$

$$\left. + \frac{\hat{t}(\bar{\tau}-\tau_g) + \hat{u}\tau_g}{\bar{\tau}(Q^2\bar{\tau}-\hat{t}\tau)\tau_g(\bar{\tau}-\tau_g)} - \frac{\hat{t}\,\hat{u}(\hat{t}+Q^2)}{\tau(Q^2\tau-\hat{t}\,\bar{\tau})^2(Q^2(\tau+\tau_g)-\hat{t}(\bar{\tau}-\tau_g))} \right) \left(\frac{e_a}{\hat{s}} - \frac{e_b}{\hat{u}} \right)$$

$$\left. - \left(\frac{Q^2\hat{t}(\bar{\tau}-\tau)}{\tau\bar{\tau}(Q^2\tau-\hat{t}\,\bar{\tau})(Q^2\bar{\tau}-\tau\hat{t})\tau_g} + \frac{1}{\bar{\tau}^2(\bar{\tau}-\tau_g)} \right) \frac{e_b}{\hat{u}} \right\}. \tag{48}$$

There is no singularity for $Q^2 \to 0$ in the amplitude for longitudinally polarized photons, the singularities (32) and (42) cancel as mentioned before. The amplitude $\mathcal{H}_{0-\lambda,0\lambda}^{P,C_F,\phi_{3\pi}}$ vanishes proportional to Q for $Q^2 \to 0$.

The complete twist-3 subprocess amplitude is given by

$$\mathcal{H}^{P,tw3} = \mathcal{H}^{P,\phi_{\pi p},reg} + \mathcal{H}^{P,q\bar{q}g,C_G} + \mathcal{H}^{P,C_F,\phi_{3\pi}}. \tag{49}$$

It meets all theoretical requirements concerning gauge invariance. For longitudinally polarized photons the three contributions in Eq. (49) vanish in the photoproduction limit as well as in the DVMP limit, see Tables I and II.

TABLE II. Power behavior of various twist-2 and twist-3 contributions for transverse and longitudinal photons for $\hat{t} \to 0$ in the generalized Bjorken regime where $\hat{s}$ and $-\hat{u}$ are of the order of Q^2.

$\mathcal{H}$	Transverse	Longitudinal
Twist-2	$\sim \frac{f_\pi}{Q} \frac{\sqrt{-\hat{t}}}{Q}$	$\sim \frac{f_\pi}{Q}$
Twist-3, 2-body, $\phi_{\pi p}$	$\sim \frac{f_\pi \mu_\pi}{Q^2}$	$\sim \frac{f_\pi \mu_\pi}{Q^2} \frac{\sqrt{-\hat{t}}}{Q}$
Twist-3, C_F, $\phi_{3\pi}$	$\sim \frac{f_{3\pi}}{Q^2}$	$\sim \frac{f_{3\pi}}{Q^2} \frac{\sqrt{-\hat{t}}}{Q}$
Twist-3, 3-body, C_G	$\sim \frac{f_{3\pi}}{Q^2}$	$\sim \frac{f_{3\pi}}{Q^2} \frac{\sqrt{-\hat{t}}}{Q}$

For nonzero $\hat{t}$ and Q^2 the propagator denominators $\tau Q^2 - \bar{\tau}\hat{t}$ and $\bar{\tau}Q^2 - \tau\hat{t}$ do not have a pole in the physical region $0 \le \tau \le 1$; see Fig. 2. Consequently, all twist-3 contributions are free from singularities generated in the end-point regions where either τ or $\bar{\tau}$ tends to zero. Possible factors $1/\tau$ or $1/\bar{\tau}$ are canceled by the end-point zeros of $\phi_{3\pi}$, i.e., $\phi_{\pi2}^{\rm EOM}$. In the limits $\hat{t} \to 0$ and $Q^2 \to 0$, however, propagator poles occur which lead to singularities in the $\phi_{\pi p}$ contribution since this DA does not vanish for $\tau \to 0$ or 1. For the photoproduction limit the singularity has already been discussed by us; see Eq. (29) and the ensuing paragraph. For the DVMP limit see Sec. III G.

F. The photoproduction limit, $Q^2 \to 0$

For later use we also quote the complete photoproduction limit of the twist-3 subprocess amplitude

$$
\begin{aligned}
\mathcal{H}_{0-\lambda,\mu\lambda}^{P,tw3} \xrightarrow{Q^2 \to 0} &\kappa_P^{(ab)} f_{3\pi}(2\lambda - \mu)\sqrt{-\hat{u}\,\hat{s}} \\
&\times \int_0^1 d\tau \int_0^{\bar{\tau}} \frac{d\tau_g}{\tau_g} \phi_{3\pi}(\tau, \bar{\tau} - \tau_g, \tau_g) \\
&\times \left[\left(\frac{1}{\bar{\tau}^2} - \frac{1}{\bar{\tau}(\bar{\tau} - \tau_g)} \right) \left(\frac{e_a}{\hat{s}^2} + \frac{e_b}{\hat{u}^2} \right) \right. \\
&\left. + \frac{C_G}{C_F} \frac{2}{\tau\tau_g} \frac{\hat{t}}{\hat{s}\,\hat{u}} \left(\frac{e_a}{\hat{s}} + \frac{e_b}{\hat{u}} \right) \right].
\end{aligned}
\tag{50}
$$

This amplitude is in agreement with the results presented in [16]. It is free of end-point singularities. The $Q^2 \to 0$ limit of the twist-2 subprocess amplitude is given in Eq. (20).

Properties of the photoproduction limit have been discussed above. The behavior of the various contributions to the subprocess for $Q^2 \to 0$ are listed in Table I.

G. The DVMP limit, $\hat{t} \to 0$

The subprocess amplitudes discussed in this section hold in any c.m.s. as well as in the limits $Q^2 \to 0$ and $\hat{t} \to 0$. The latter limit is the region of DVMP where factorization of the leading-twist contribution has been shown to hold for large Q^2 [2], for instance in Ji's frame [34]. In this frame in which skewness is nonzero, $\hat{s}$ and $\hat{u}$ are related to Q^2 by
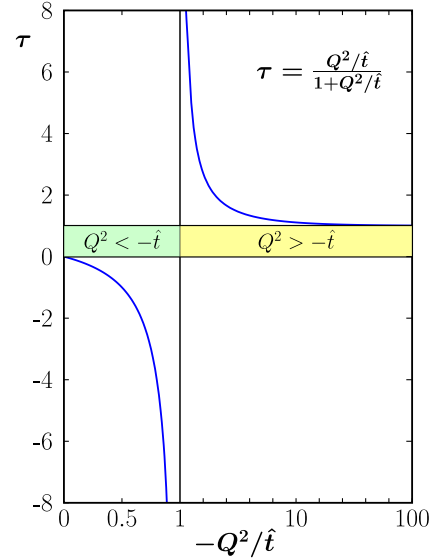

FIG. 2. The function $\tau = \frac{Q^2/\hat{t}}{1+Q^2/\hat{t}}$. For $-Q^2/\hat{t} > 1$ a logarithmic scale is used.

$$
\hat{s} = \frac{x - \xi}{2\xi} Q^2, \qquad \hat{u} = -\frac{x + \xi}{2\xi} Q^2,
\tag{51}
$$

i.e., $\hat{s}$ and $\hat{u}$ are of order of Q^2. The behavior of the various contributions to the subprocess amplitudes for $\hat{t} \to 0$ are compiled in Table II. One sees from that table that the asymptotically dominant contribution comes from longitudinally polarized photons at the twist-2 level. In fact, the $\hat{t} \to 0$ limit of (18) is the familiar LO, leading-twist result [2]. On the other hand, the transverse leading-twist amplitude vanishes proportional to $\sqrt{-\hat{t}}$ and, compared to the longitudinal amplitude, is suppressed by $1/Q$. Table II also reveals that all twist-3 contributions for longitudinally polarized photons vanish $\sim\sqrt{-\hat{t}}$ as a consequence of angular momentum conservation. The twist-3 contributions for transversely polarized photons remain finite for $\hat{t} = 0$ but are suppressed by μ_π/Q or $f_{3\pi}/Q$ compared to the dominant twist-2 contribution for longitudinally polarized photons.

It is also informative to see the twist-3 subprocess amplitudes in the DVMP limit:

$$
\begin{aligned}
\mathcal{H}_{0-\lambda,\mu\lambda}^{P,\phi_{\pi p}} \xrightarrow{\hat{t} \to 0} &(2\lambda + \mu)\kappa_P^{(ab)} f_\pi \mu_\pi \sqrt{-\frac{\hat{u}}{\hat{s}}} \left[\frac{e_a}{\hat{s}} + \frac{\hat{s}}{\hat{u}} \frac{e_b}{\hat{u}} \right] \int_0^1 \frac{d\tau}{\bar{\tau}} \phi_{\pi p}(\tau), \\
\mathcal{H}_{0-\lambda,\mu\lambda}^{P,q\bar{q}g,C_G} \xrightarrow{\hat{t} \to 0} &(2\lambda + \mu)\kappa_P^{(ab)} f_{3\pi} \left(1 - \frac{1}{2}\frac{C_A}{C_F} \right) \frac{Q^2}{\sqrt{-\hat{s}\,\hat{u}}} \left(\frac{e_a}{\hat{s}} + \frac{e_b}{\hat{u}} \right) \int_0^1 \frac{d\tau}{\bar{\tau}} \int_0^{\bar{\tau}} \frac{d\tau_g}{\tau_g(\bar{\tau} - \tau_g)} \phi_{3\pi}(\tau, \bar{\tau} - \tau_g, \tau_g), \\
\mathcal{H}_{0-\lambda,\mu\lambda}^{P,C_F,\phi_{3\pi}} \xrightarrow{\hat{t} \to 0} &- (2\lambda + \mu)\kappa_P^{(ab)} f_{3\pi} \sqrt{-\frac{\hat{u}}{\hat{s}}} \left(\frac{e_a}{\hat{s}} + \frac{\hat{s}}{\hat{u}} \frac{e_b}{\hat{u}} \right) \int_0^1 \frac{d\tau}{\bar{\tau}^2} \int_0^{\bar{\tau}} \frac{d\tau_g}{\tau_g(\bar{\tau} - \tau_g)} \phi_{3\pi}(\tau, \bar{\tau} - \tau_g, \tau_g).
\end{aligned}
\tag{52}
$$

In the DVMP limit only the helicity nonflip amplitude $\mathcal{H}_{0-,++}^{P,tw3}$ is left over while $\mathcal{H}_{0-,-+}^{P,tw3}$ vanishes $\propto \hat{t}$ as a consequence of angular momentum conservation. Thus, a full twist-3 DVMP analysis modifies the WW approximation employed in [10,11] by a change of the DA $\phi_{\pi p}$ generated through the 3-body DA via the equation of motion (21) and by the additional 3-body contributions. From the properties of the 3-body DA, $\phi_{3\pi}$ [see Eq. (55)], it is clear that the 3-body contributions[5] given in (52) do not have end-point singularities. On the other hand, the $\phi_{\pi p}$ contribution possesses an end-point singularity since this DA does not vanish at the end points as we already remarked. This singularity has been regularized in [10,11] by keeping the quark transverse momentum in the propagators. More details on the twist-3 contribution in the DVMP limit will be given in a forthcoming paper [35].

IV. DAs, FORM FACTORS AND PARAMETERS

For the soft physics input to our calculation of pion electroproduction we use the same DAs and form factors as for π^0 photoproduction [16]. Thus, for the twist-2 pion DA we use the truncated Gegenbauer expansion

$$\phi_\pi(\tau) = 6\tau\bar{\tau}[1 + a_2 C_2^{3/2}(2\tau - 1)], \qquad (53)$$

with the recent lattice QCD result on the second Gegenbauer coefficient [36]

$$a_2(\mu_0) = 0.1364 \pm 0.0213 \qquad (54)$$

at the initial scale $\mu_0 = 2$ GeV. The coefficient a_2 as all other expansion coefficients depend on the factorization scale, μ_F, which is defined by (16). The corresponding anomalous dimensions are quoted in the Appendix.

For the 3-body twist-3 DA we follow [31] and use the truncated conformal expansion

$$\phi_{3\pi}(\tau_a, \tau_b, \tau_g) = 360\tau_a\tau_b\tau_g^2\left[1 + \omega_{1,0}\frac{1}{2}(7\tau_g - 3)\right.$$

$$+ \omega_{2,0}(2 - 4\tau_a\tau_b - 8\tau_g + 8\tau_g^2)$$

$$\left. + \omega_{1,1}(3\tau_a\tau_b - 2\tau_g + 3\tau_g^2)\right], \qquad (55)$$

with

$$\omega_{10}(\mu_0) = -2.55, \qquad \omega_{20}(\mu_0) = 8.0, \qquad \omega_{11}(\mu_0) = 0.0. \qquad (56)$$

The coefficients ω_{20} and ω_{11} mix under evolution; see the Appendix. The 3-body DA is normalized as

---

[5]Note that the 2-body twist-3 contribution proportional to $\phi_{\pi 2}^{EOM}$ and contributing to $\mathcal{H}^{P,C_F,\phi_{3\pi}}$ vanishes for $\hat{t} \to 0$.

$$\int_0^1 d\tau \int_0^{\bar{\tau}} d\tau_g \phi_{3\pi}(\tau, \bar{\tau} - \tau_g, \tau_g) = 1. \qquad (57)$$

For the parameter $f_{3\pi}$ we take

$$f_{3\pi}(\mu_0) = 0.004 \text{ GeV}^2. \qquad (58)$$

This parameter as well as the expansion coefficient ω_{10} have been derived from QCD sum rules [29]. According to [29] the uncertainties of these parameters are large of the order of 30%. The expansion coefficient ω_{20} has been adjusted by us [16] to the CLAS data on π^0 photoproduction [15].

Using (55), we obtain the function $\phi_{\pi 2}^{EOM}$ from the integral (22)

$$\phi_{\pi 2}^{EOM}(\tau) = 120\frac{f_{3\pi}}{f_\pi\mu_\pi}\tau(1-\tau)^3\left[1 + \frac{1}{4}\omega_{1,0}(1-7\tau)\right.$$

$$\left. + \frac{2}{5}\omega_{2,0}(1 - 7\tau + 11\tau^2) - \frac{1}{10}\omega_{1,1}(1 - 7\tau + 6\tau^2)\right]. \qquad (59)$$

The equations of motion (21) can be suitably combined and solved for $\phi_{\pi p}$ and $\phi_{\pi\sigma}$ [16]:

$$\phi_{\pi\sigma}(\tau) = 6\tau\bar{\tau}\left(\int d\tau \frac{\bar{\tau}\phi_{\pi 2}^{EOM}(\bar{\tau}) - \tau\phi_{\pi 2}^{EOM}(\tau)}{2\tau^2\bar{\tau}^2} + C\right),$$

$$\phi_{\pi p}(\tau) = \frac{1}{6\tau\bar{\tau}}\phi_{\pi\sigma}(\tau) + \frac{1}{2\tau}\phi_{\pi 2}^{EOM}(\bar{\tau}) + \frac{1}{2\bar{\tau}}\phi_{\pi 2}^{EOM}(\tau). \qquad (60)$$

The constant of integration, C, is fixed from the constraint

$$\int_0^1 d\tau \phi_{\pi p}(\tau) = 1. \qquad (61)$$

Thus, for a given 3-body DA, $\phi_{3\pi}$, the 2-body twist-3 DAs are uniquely fixed. Since we started from a truncated expansion of $\phi_{3\pi}$ we arrive at truncated Gegenbauer expansions of the 2-body twist-3 DAs [16] (the C_n^m denote the Gegenbauer polynomials):

$$\phi_{\pi p}(\tau) = 1 + \frac{1}{7}\frac{f_{3\pi}}{f_\pi\mu_\pi}(7\omega_{1,0} - 2\omega_{2,0} - \omega_{1,1})$$

$$\times (10C_2^{1/2}(2\tau - 1) - 3C_4^{1/2}(2\tau - 1)). \qquad (62)$$

The DA $\phi_{\pi\sigma}$ is not needed by us in this work explicitly. Thus, we refrain from quoting it here. It can be found in [16]. If $\phi_{3\pi} = 0$ Eq. (60) reduces to the well-known WW approximation of the DAs

$$\phi_{\pi p}^{WW} = 1, \qquad \phi_{\pi\sigma}^{WW} = 6\tau\bar{\tau}. \qquad (63)$$

Let us now turn to the discussion of the form factors, $F_i^P(t)(= R_i^P(t), S_i^P(t))$ which encode the soft physics content of the nucleon matrix element. The form factors are

given by process specific combinations of the corresponding flavor form factors, F_i^a, which are defined as $1/x$-moments of zero-skewness GPDs, K_i^a,

$$F_i^a(t) = \int_0^1 \frac{dx}{x} K_i^a(x, t). \quad (64)$$

Here, $x = (k_j + k_j')^+/(p + p')^+$ is the average momentum fraction the two active quarks carry and a is a valence quark. The restriction to valence quarks is an assumption for charged pions which will be justified at the end of this section. For π^0-production this restriction is a consequence of charge-conjugation parity.

The usual GPDs, K_i, parametrize the soft proton-proton matrix elements. However, for electroproduction of charged pions proton-neutron transition matrix elements appear. With the help of SU(3) flavor symmetry these transition GPDs and, hence, the corresponding form factors, can be related to the diagonal proton-proton ones [37]:

$$\gamma^* p \rightarrow \pi^+ n \colon F_i^{\pi^+}(t) = F_{ip \rightarrow n}(t) = F_i^u(t) - F_i^d(t),$$
$$\gamma^* n \rightarrow \pi^- p \colon F_i^{\pi^-}(t) = F_{in \rightarrow p}(t) = F_i^u(t) - F_i^d(t). \quad (65)$$

For π^0 production there are two subprocesses $\gamma^* u \rightarrow \pi^0 u$ and $\gamma^* d \rightarrow \pi^0 d$. In both cases $e_a = e_b$. It is therefore convenient to pull out the charges from the subprocess amplitudes for this process and to absorb them into the form factors together with the corresponding flavor weight factors (13). Thus, the form factors specific to π^0 production read

$$F_i^{\pi^0}(t) = \frac{1}{\sqrt{2}} [e_u F_i^u(t) - e_d F_i^d(t)]. \quad (66)$$

Consequently, the subprocess amplitudes do not depend anymore on the flavors in the case of π^0 production.

In [6] the GPDs H and E for valence quarks have been extracted from the data on the magnetic and electric form factors of the nucleon exploiting the sum rules for the form factors with the help of a parametrization of the zero skewness GPDs

$$K_i^a = k_i^a(x) \exp [t f_i^a(x)]. \quad (67)$$

In [5,6] it is advocated for the following parametrization of the profile function[6]

$$f_i^a(x) = (B_i^a - \alpha_i'^a \ln x)(1 - x)^3 + A_i^a x(1 - x)^2, \quad (68)$$

with the parameters A_i, B_i and α_i fitted to the data of the nucleon's electromagnetic form factors. The forward limit of the GPD H^a is given by the flavor-a parton density,

---

[6]This ansatz is now supported by light-front holographic QCD [38]. A similar parametrization has been proposed in [39].

$q^a(x)$ which is taken from [40]. Since the forward limit of E^a is not accessible in deep-inelastic scattering it is, therefore, to be determined in the form factor analysis, too. The most prominent feature of the GPDs, parametrized as in (67) and (68), is the strong $x - t$ correlation [5,6]: The GPDs at small x control the behavior of their associated flavor form factors at small $-t$ whereas large x determine their large $-t$ behavior. The flavor form factors R_V^a and R_T^a are evaluated from the GPDs (67), (68). These flavor form factors have also been used in wide-angle Compton scattering [6].

For the form factor, R_A, being related to the GPD $\tilde{H}$, we use example #1 discussed in [41]. This example is extracted from the data on the axial form factor of the nucleon and on the helicity correlations, A_{LL} and K_{LL}, measured in wide-angle Compton scattering [42,43].

For the transversity GPDs H_T and $\bar{E}_T$ the parametrization (67), (68) is also employed and the parameters, B_i^a and $\alpha_i'^a$, fixed from the low $-t$ data on deeply virtual pion electroproduction [10,11]. The values of these parameters can be found in [16]. For wide-angle photo- and electro-production the large $-t$ behavior, i.e., the second term in the profile function, is also required. As in [16] we use for the relevant parameter A_i^a the value 0.5 GeV^2 for all transversity GPDs. With this choice a good fit to the CLAS data [15] on π^0 photoproduction has been obtained. At present there is no information available on the GPD $\tilde{H}_T$ and its associated from factor S_S. In order to have an at least rough estimate of its importance we assume, with regard to the definition of the GPD $\bar{E}_T$

$$\bar{E}_T = 2\tilde{H}_T + E_T, \quad (69)$$

that $S_S^a = \bar{S}_T^a/2$. This assumption is equivalent to the neglect of E_T.

Last, but not least, we want to discuss a property of the GPDs (67), (68) which is of particular significance for exclusive wide-angle processes. With the help of the saddle point method [5] one can show that moments of these GPDs, fall as a power of t at large $-t$:

$$F_i^a \sim 1/(-t)^{d_i^a}, \quad (70)$$

where

$$d_i^a = (1 + \beta_i^a)/2, \quad (71)$$

and β_i^a is the power of $1 - x$ with which the forward limit of the GPD K_i^a vanishes for $x \rightarrow 1$. Equation (70) is a generalization of the famous Drell-Yan relation [44]. The phenomenological values of the powers d_i^a are listed in Table III. Note the differences between the powers of u and d-quarks. This implies that at very large $-t$ only u-quark flavor form factors contribute. In case of the helicity nonflip GPDs the powers β_i^u are slightly larger than expected

TABLE III. The powers d_i for the form factors contributing to the wide-angle photo- and electroproduction of pions. The table is taken from ref. [16].

	R_V^a	R_A^a	R_T^a	S_T^a	$\bar{S}_T^a$
u	2.25	2.22	2.83	2.5	2.5
d	3.0	2.61	3.12	3.5	3.0

according to perturbative QCD arguments [45,46]. We however stress that, in practice, the powers, β_i^a, are fixed in a region of x less than about 0.8 for the helicity nonflip GPDs, and even a smaller x-region for the transversity ones. For larger x there is no experimental information on the forward limits available at present. Therefore, the powers β_i^a are to be considered as effective powers which are likely subject to changes as soon as data at larger x become available. These powers affect the energy dependence of the cross sections. For photoproduction the energy dependence of the cross section at fixed $\cos\theta$ can readily be read off from (9) and the subprocess amplitudes discussed in Sec. III. One finds the familiar $1/s^7$ scaling behavior of the cross section at fixed $\cos\theta$ for the twist-2 contribution and $1/s^8$ for the twist-3 one provided the form factors, including the prefactors of $\sqrt{-t}$ and t appearing in (9), drop as $1/t^2$. Deviations from that behavior change the scaling behavior as do the logs from α_s and the evolution of the DA parameters. As can be seen from Table III our form factors increase the power of s with which the cross section falls. In the energy range we explore the effective scaling is $1/s^9$.

As is well-known the sea-quark densities fall faster to zero for $x \to 1$, typically as $\sim(1-x)^7$ than the valence quark densities; see for instance [40]. This is also expected from perturbative QCD arguments [45]. The forward limits of the other GPDs may fall even more rapidly than

that of H^{sea}. According to (70) the sea-quark form factor falls as

$$R_V^{\text{sea}}(t) \sim 1/(-t)^4. \tag{72}$$

The other sea-quark form factors decrease like R_V^{sea} or even faster. Thus, we conclude that sea-quark contributions to wide-angle electroproduction are strongly suppressed and therefore neglected by us.

V. PHOTOPRODUCTION

The photoproduction cross section

$$\frac{d\sigma^P}{dt} = \frac{1}{32\pi(s-m^2)^2} \sum_{\nu'\mu} |\mathcal{M}_{0\nu',\mu+}^P|^2 \tag{73}$$

is evaluated from (9) using the subprocess amplitudes (20) and (50) as well as the DAs and form factors described in Sec. IV. The resulting cross sections for the various pion channels, scaled by s^7 in order to take away most of the energy dependence, are displayed in Figs. 3 and 4 as solid lines and compared to experiment [15,21,47]. Of course, there is agreement with the CLAS data [15] since the expansion coefficient ω_{20} is fitted to these data. On the other hand, there is substantial disagreement with the SLAC data [21]. In particular the SLAC π^0 data are about an order of magnitude larger than the new CLAS data in the vicinity of 90 degrees. With regard to the prerequisite of the handbag approach that the Mandelstam variables should be much larger than the hadronic scale, Λ^2, we only show results for $-t$ and $-u$ larger than 2.5 GeV². This is a compromise between the requirement of the handbag approach, on the one side, and having available a not too small range of $\cos\theta$ for the experimentally accessible values of s on the other side.
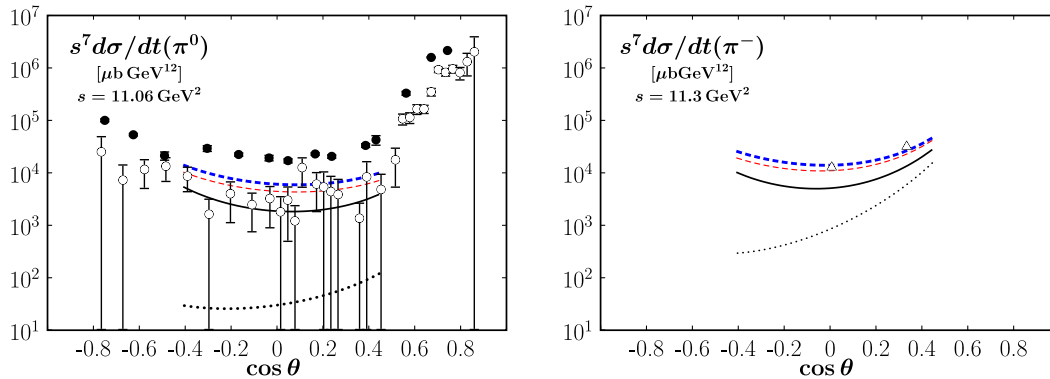

FIG. 3. Left: The cross section for π^0 photoproduction versus the cosine of the c.m.s. scattering angle, θ, at $s = 11.06$ GeV². The solid (dotted) curve represents the full (twist 2) result using the same parameters as in [16]. The red dashed curve is obtained with the same parameters as in [16] but with the amplitudes taken at the fixed scale $\mu_R = \mu_F = 1$ GeV, while for the blue dashed curve we additionally change $\omega_{20} = 10.3$. Data taken from [21] (full circles) at $s = 10.3$ GeV² and from CLAS [15] (open circles) at $s = 11.06$ GeV². The cross sections are scaled by s^7 and the theoretical results are only shown for $-t$ and $-u$ larger than 2.5 GeV². Right: Results for the π^- photoproduction cross section at $s = 11.3$ GeV². Data, shown as open triangles, are from [47]. For other notations it is referred to the figure on the left hand side.

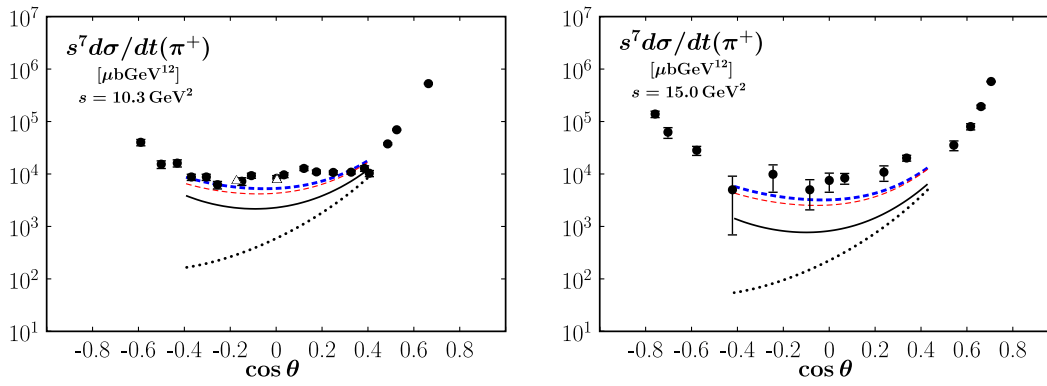FIG. 4. Results for the π^+ photoproduction cross sections vs $\cos\theta$, at $s = 10.3$ GeV^2 (left) and 15 GeV^2 (right). The full circles are the data from [21] at $s = 10.3$ and 15 GeV^2; the open triangles are from [47] at $s = 11.3$ GeV^2. At $s = 15$ GeV^2 results are shown for $-t$ and $-u$ larger than 4 GeV^2. For other notations it is referred to Fig. 3.

The corresponding results for the $\pi^\pm$ cross sections are shown in Figs. 3 and 4 and compared to the SLAC [21] and Jefferson Lab Hall A data [47]. For positive values of $\cos\theta$ theory and experiment are close to each other but near 90 degrees and in the backward hemisphere our results are well below the data [21,47] (by a factor of 2 to 3). In contrast to π^0 photoproduction the twist-2 contribution to the $\pi^\pm$ cross section is substantial in the forward hemisphere; see Figs. 3 and 4. This can be understood from properties of the subprocess amplitude (20):

$$\frac{\mathcal{H}^{\pi^\pm}}{\mathcal{H}^{\pi^0}} \sim \frac{e_a \hat{u} + e_b \hat{s}}{\hat{s} + \hat{u}}. \tag{74}$$

This ratio is large for small $-\hat{t} = -\hat{s} - \hat{u}$. With rising $-t$, i.e., decreasing $\cos\theta$, the twist-3 contribution quickly takes the lead. The twist-2—twist-3 interference is however noticeable in the entire wide-angle region even for π^0 photoproduction. At $\cos\theta \simeq -0.4$ the interference term still amounts to about 10%, positive for π^+ production and negative for the case of π^-. With increasing s the twist-2 contribution becomes more important (see Fig. 4) since, as is evident from Table I, the twist-3 subprocess amplitude is suppressed by an extra factor $1/\sqrt{\hat{s}}$.

The π^- photoproduction cross section is larger than the π^+ one by a factor $2 - 3$. The reason for this fact are the quark-charge factors in (20) and (50) which favor the π^- channel [$n = 1, 2$, see (50)]

$$\frac{\mathcal{H}^{\pi^-}}{\mathcal{H}^{\pi^+}} \sim \frac{e_d \hat{u}^n + e_u \hat{s}^n}{e_u \hat{u}^n + e_d \hat{s}^n}. \tag{75}$$

The absolute value of this ratio is larger than 1.

The discrepancy between theory and experiment is larger at $s = 15$ GeV^2 than at 10.3 GeV^2. It seems that the predicted energy dependence is too strong. It also seems that the ratio of the π^- and π^+ cross sections at 90° is too large as compared to the Hall A data [47]. Some fine tuning

of the soft-physics input is perhaps necessary. We however hesitate to do so since the SLAC data are very old and a remeasurement of wide-angle $\pi^\pm$ photoproduction seems to be advisable.

At the end of Sec. IV we already discussed the energy dependence of the handbag approach. As we mentioned in Sec. IV, in the range of s we are interested in, our cross section effectively behaves $\propto s^{-9}$ in the region of twist-3 dominance. This is perhaps somewhat too strong. Since our form factors represent $1/x$-moments of GPDs they evolve with the scale in principle. Because of the strong $x - t$ correlation the form factors at large $-t$ are under control of a narrow region of large x. With increasing $-t$ the affected region approaches 1 and becomes narrower. Therefore, our form factors approximately become equal to the scale-independent lowest moments of the GPDs concerned. Thus, as it is argued in [5], the $1/x$-factors in the form factors can be viewed as a phenomenological estimate of effects beyond the strict $\Lambda/\sqrt{-t}$ expansion (see Sec. II). One may likewise argue that the disregard of the scale-dependence of the form factors also requires the neglect of the evolution of the DAs for consistency. Thus, as already discussed in [16], we also evaluate the photoproduction cross sections at the fixed scale of $\mu_R = \mu_F = 1$ GeV as an alternative and fit the coefficient ω_{20} to the CLAS and SLAC data. This procedure hardly alters the size and shape of the cross sections but reduces their effective energy dependence to about s^{-8} in regions of twist-3 dominance. The results we obtain with the fixed scale are shown as dashed lines in Fig. 3: red for the usual parameters taken form [16] and blue for $\omega_{20} = 10.3$. They agree fairly well with the data and one notes that freezing the scale has bigger effect than changing ω_{20}.

VI. ELECTROPRODUCTION

As is well known, for pion electroproduction there are four partial cross sections in contrast to just Eq. (73) for photoproduction. For the ease of access we repeat the
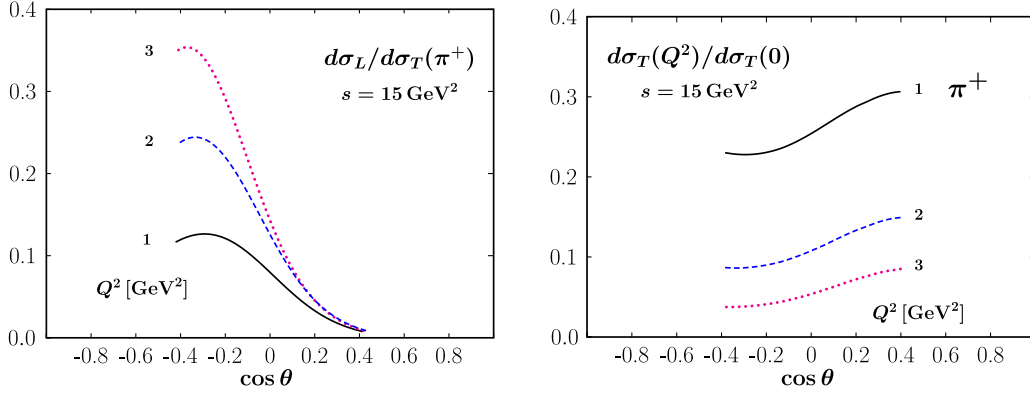
FIG. 5.   Left: Predictions for the ratio of the longitudinal and transverse cross sections for π^+ electroproduction versus the cosine of the c.m.s. scattering angle at $s = 15$ GeV^2 for a set of Q^2 values. Parameters as in [16]. The predictions are only shown for $-\hat{t}$ and $-\hat{u}$ larger than 4 GeV^2. Right: As the figure on the left hand side but for the ratio of the transverse and the photoproduction cross sections.

definitions of the partial cross sections in terms of helicity amplitudes

$$\frac{d\sigma_L}{dt} = 2\varrho_{ps}[|\mathcal{M}_{0+,0+}|^2 + |\mathcal{M}_{0-,0+}|^2],$$

$$\frac{d\sigma_T}{dt} = \varrho_{ps}\sum_\mu[|\mathcal{M}_{0+,\mu+}|^2 + |\mathcal{M}_{0-,\mu+}|^2],$$

$$\frac{d\sigma_{LT}}{dt} = -\sqrt{2}\varrho_{ps}\mathrm{Re}\sum_\mu\mu[\mathcal{M}^*_{0-,0+}\mathcal{M}_{0-,\mu+} + \mathcal{M}^*_{0+,0+}\mathcal{M}_{0+,\mu+}],$$

$$\frac{d\sigma_{TT}}{dt} = -2\varrho_{ps}\mathrm{Re}[\mathcal{M}^*_{0-,++}\mathcal{M}_{0-,-+} + \mathcal{M}^*_{0+,++}\mathcal{M}_{0+,-+}],$$

$$(76)$$

where the phase space factor is given by

$$\varrho_{ps} = \left[32\pi(s - m^2)\sqrt{\Lambda_M(s, -Q^2, m^2)}\right]^{-1}, \quad (77)$$

where Λ_M is the Mandelstam function.[7]

The partial cross sections sum up to the unpolarized $ep \rightarrow e\pi N$ cross section:

$$\frac{d^4\sigma}{dsdQ^2dtd\varphi} = \frac{\alpha_{\mathrm{em}}(s - m^2)}{16\pi^2 E_L^2 m^2 Q^2(1-\varepsilon)}\left(\frac{d\sigma_T}{dt} + \varepsilon\frac{d\sigma_L}{dt}\right.$$

$$\left. + \varepsilon\cos(2\varphi)\frac{d\sigma_{TT}}{dt} + \sqrt{2\varepsilon(1+\varepsilon)}\cos\varphi\frac{d\sigma_{LT}}{dt}\right).$$

$$(78)$$

Here, φ is the azimuthal angle between the lepton and the hadron plane and E_L is the energy of the lepton beam. The ratio of the longitudinal and transversal photon flux is denoted by ε.

---

[7]In DVMP s is usually denoted by W^2.

The twist-2 and twist-3 subprocess amplitudes for pion electroproduction are presented in Sec. III. From these subprocess amplitudes in combination with the form factors described in Sec. IV, we evaluate the amplitudes (9), (11) and subsequently the partial cross sections (76). In the light of the discussion in the preceding section we will mostly show ratios of cross sections for pion electroproduction. Most of the energy dependence and of the normalization uncertainties cancel in the ratios. Therefore, we only show results evaluated from the same DAs and flavor form factors as in [16].

First, we compare the partial cross sections for, say, π^+ production for different photon virtualities. In order to have at disposal a rather large range of Q^2 we need large $-t$ and $-u$ because of the requirement (1) and consequently large s. Therefore, we choose the not unrealistically large value of 15 GeV^2 for s and show the partial cross sections only for $Q^2 = 1, 2$ and 3 GeV^2 and $-t, -u \geq 4$ GeV^2. In Fig. 5 we present the ratio of the longitudinal and the transverse cross section as well as the ratio of the transverse and the photoproduction cross section for $Q^2 = 1, 2$ and 3 GeV^2. The interference cross sections, divided by the transverse one, are displayed in Fig. 6. The ratios reveal a mild $\cos\theta$ and Q^2-dependence. The latter one is getting only somewhat stronger in the backward hemisphere.

In Fig. 7 we show the separate longitudinal and transverse cross sections versus Q^2 at $\cos\theta = 0$. Starting at zero in the photoproduction limit the longitudinal cross section increases with rising Q^2 up to a maximum at about 1.0 GeV^2 while the transverse cross sections for charge pions are continuously decreasing. The π^0 cross section has a mild minimum at about $Q^2 = 0.7$ GeV^2. The magnitudes of the longitudinal cross sections differ markedly. The π^+ cross section is very small compared to the other ones. As for photoproduction, see Eq. (75), the quark charges favor the π^- production over the π^+ one.
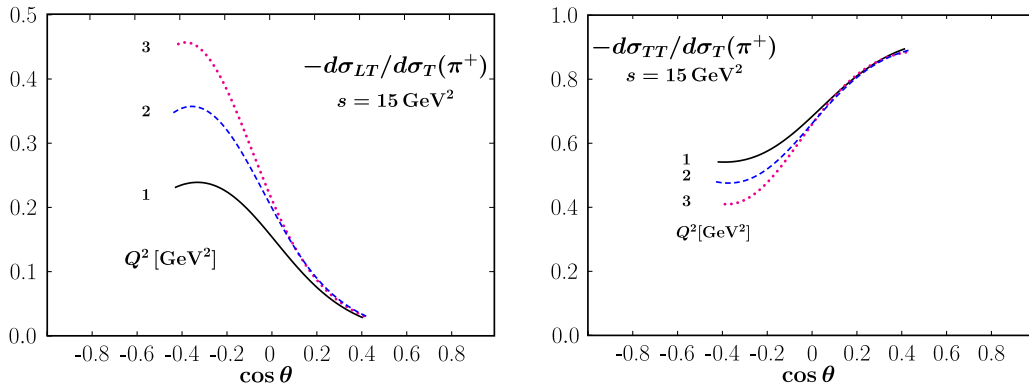
FIG. 6. Predictions for the longitudinal-transverse (left) and transverse-transverse (right) interference cross sections of π^+ electroproduction divided by the transverse one versus the cosine of the c.m.s. scattering angle at $s = 15$ GeV^2 for a set of photon virtualities.
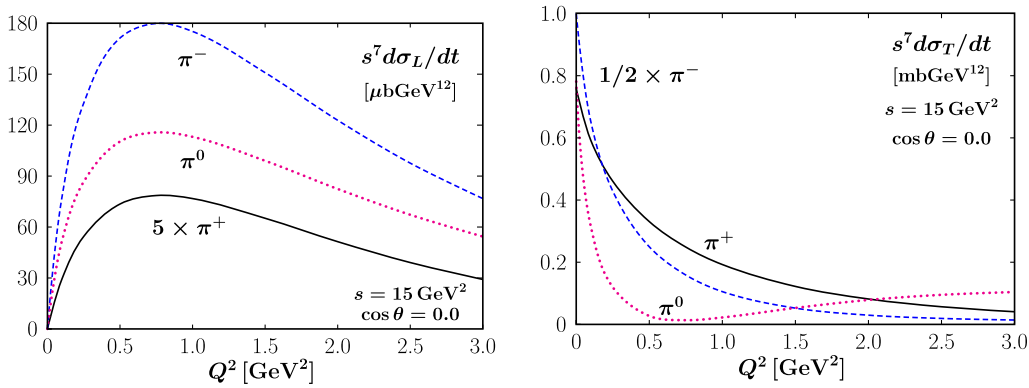

FIG. 7. Predictions for the longitudinal (left) and the transverse (right) cross sections of π^+ (solid), π^- (dashed) and π^0 (dotted line) electroproduction versus Q^2 at $s = 15$ GeV^2 and $\cos\theta = 0$. Parameters as in [16].

In Figs. 8 and 9 the partial cross sections for the three pion channels are shown at $s = 10.3$ GeV^2 and at a fixed Q^2 of 2 GeV^2. As in Figs. 5 and 6 the partial cross sections are divided by the transverse one except of the transverse cross section itself which is divided by the corresponding photoproduction cross section. The cross sections for the various pions differ markedly from each other. Particularly noteworthy are the maxima in the partial cross sections
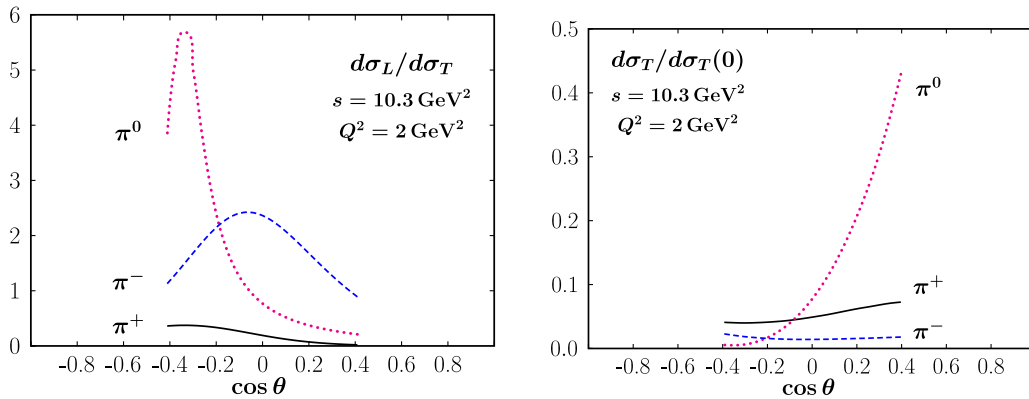

FIG. 8. Predictions for the ratio of the longitudinal and transverse cross sections (left) and the transverse cross sections divided by the photoproduction one (right) of pion electroproduction vs $\cos\theta$ at $s = 10.3$ GeV^2 and $Q^2 = 2.0$ GeV^2. Parameters as in [16]. The predictions are only shown for $-\hat{t}$ and $-\hat{u}$ larger than 2.5 GeV^2.
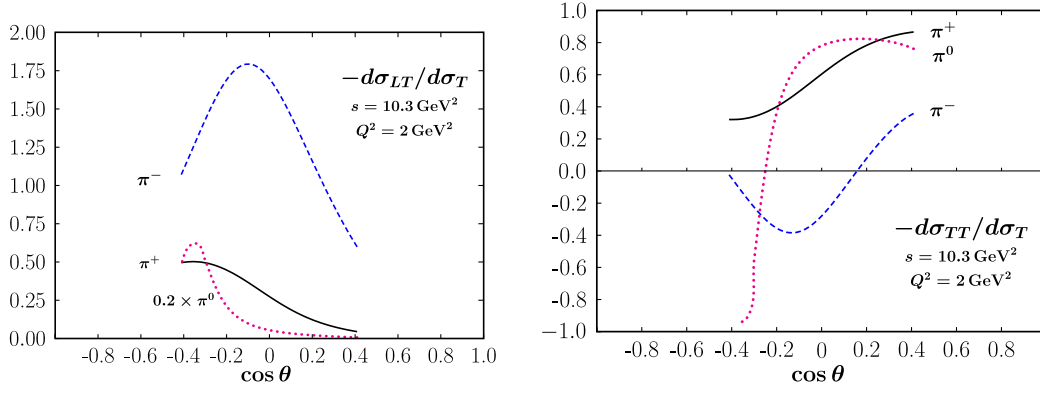
FIG. 9. Predictions for the longitudinal-transverse (left) and transverse-transverse (right) interference cross sections of pion electroproduction vs $\cos\theta$ at at $s = 10.3$ GeV^2 and $Q^2 = 2.0$ GeV^2. The interference cross sections are divided by the corresponding transverse cross section.

occurring near 90 degrees for π^- and at about 115 degrees for π^0 production. The sharp peak of the ratio of $d\sigma_L$ and $d\sigma_T$, especially for the case of π^0 production, is generated by a conspiracy of minima at slightly different positions and dissimilar depths of these cross sections. Comparison of the π^+-curves in Figs. 8 and 9 with the $Q^2 = 2$ GeV^2 curves in Figs. 5 and 6 gives an impression of the energy dependence of pion electroproduction.

Data on the partial cross section of pion electroproduction will allow for an extraction of detailed information on the large $-t$-behavior of the transversity GPDs. Thus, as is evident from (11), the longitudinal cross section is only dependent upon the form factors $(R_A^P)^2$ and $(S_T^P)^2$; there is no interference between the twist-2 and twist-3 contributions. As a little calculation reveals, the longitudinal-transverse interference cross section has the same structure:

$$\frac{d\sigma_{LT}^P}{dt} = -\sqrt{2}e_0^2\varrho_{ps}[\mathcal{H}_{0+,0+}^P(\mathcal{H}_{0+,++}^P - \mathcal{H}_{0+,-+}^P)(R_A^P)^2 + \mathcal{H}_{0-,0+}^P(\mathcal{H}_{0-,++}^P - \mathcal{H}_{0-,-+}^P)(S_T^P)^2]. \quad (79)$$

Given that the axial form factor, R_A^P, is not unknown at large $-t$, from data on the longitudinal and the longitudinal-transverse cross sections we may extract information on S_T^P and thus on H_T from data on the longitudinal and the longitudinal-transverse interference cross sections. The transverse as well as the transverse-transverse interference cross sections depend on all six form factors and, hence, on the form factor S_S^P too. This form factor represents the $1/x$-moment of the completely unknown transversity GPD $\tilde{H}_T$. In DVMP this GPD is strongly suppressed since it comes together with the factor $t/(4m^2)$. Numerical examination laid open that $d\sigma_{TT}^P$ is very sensitive to S_S^P in the regions of twist-3 dominance. Thus, it seems that a measurement of $d\sigma_{TT}^P$ may provide information on $\tilde{H}_T$ at least at large $-t$.

VII. SPIN EFFECTS

The derivation of the photo- and electroproduction amplitudes within the handbag approach naturally requires the use of the light-cone helicity basis. However, for comparison with experimental results on spin-dependent observables, the use of ordinary photon-nucleon c.m.s. helicity amplitudes is more convenient. The ordinary helicity amplitudes, $\Phi_{0\nu',\mu\nu}$, are obtained from the light-cone ones (9), by the transform (see [48–50])

$$\Phi_{0\nu',\mu\nu}^P = \mathcal{M}_{0\nu',\mu\nu}^P$$
$$+ (-1)^{1/2+\nu'}\kappa'\mathcal{M}_{0-\nu',\mu\nu}^P$$
$$+ (-1)^{1/2+\nu}\kappa\mathcal{M}_{0\nu',\mu-\nu}^P + \mathcal{O}(m^2/s),$$
$$\Phi_{0\nu',0\nu}^P = \mathcal{M}_{0\nu',0\nu}^P + (-1)^{1/2+\nu'}(\kappa'+\kappa)\mathcal{M}_{0-\nu',0\nu}^P$$
$$+ \mathcal{O}(m^2/s), \quad (80)$$

where

$$\kappa = \frac{m}{s+Q^2}\sqrt{s+Q^2/2}\frac{\sin\vartheta}{1+\cos\vartheta},$$
$$\kappa' = -\kappa\left(1 - \frac{Q^2}{4s} - \frac{Q^2}{s}\frac{\cos\vartheta}{1-\cos\vartheta}\right). \quad (81)$$

For convenience the notation of the helicities is kept and the angle ϑ is defined in (4). In the photoproduction limit κ' becomes $-\kappa$ and

$$\kappa \overset{Q^2\to 0}{\longrightarrow} \frac{m}{\sqrt{s}}\frac{\sqrt{-t}}{\sqrt{s}+\sqrt{-u}}. \quad (82)$$

Obviously,

$$\sum_{\nu',\mu} |\Phi_{0\nu',\mu+}^P|^2 = \sum_{\nu',\mu} |\mathcal{M}_{0\nu',\mu+}^P|^2,$$

$$\sum_{\nu'} |\Phi_{0\nu',0+}^P|^2 = \sum_{\nu'} |\mathcal{M}_{0\nu',0+}^P|^2. \tag{83}$$

A. Helicity correlations in photoproduction

As for wide-angle Compton scattering the most interesting spin-dependent observables of pion photoproduction are the correlations of the helicities of the incoming photon and that of either the incoming or the outgoing nucleon, A_{LL}, or K_{LL}, respectively. In terms of helicity amplitudes these observables are defined by

$$A_{LL}^P = \frac{|\Phi_{0+,++}^P|^2 - |\Phi_{0+,-+}^P|^2 + |\Phi_{0-,++}^P|^2 - |\Phi_{0-,-+}^P|^2}{\sum_{\nu',\mu} |\Phi_{0\nu',\mu+}^P|^2},$$

$$K_{LL}^P = \frac{|\Phi_{0+,++}^P|^2 - |\Phi_{0+,-+}^P|^2 - |\Phi_{0-,++}^P|^2 + |\Phi_{0-,-+}^P|^2}{\sum_{\nu',\mu} |\Phi_{0\nu',\mu+}^P|^2}. \tag{84}$$

One can easily check that for the twist-3 contribution one has

$$A_{LL}^{P,tw3} = -K_{LL}^{P,tw3}, \tag{85}$$

while for twist 2

$$A_{LL}^{P,tw2} = K_{LL}^{P,tw2} \tag{86}$$

holds as is the case for wide-angle Compton scattering [41,50]. Thus, the experimental observation of an approximate mirror symmetry between A_{LL}^P and K_{LL}^P signals the dominance of twist-3 contributions to pion photoproduction. With regard on that feature A_{LL}^P and K_{LL}^P play a similar important role for the discrimination between twist 2

and twist 3 in photoproduction of pions as the longitudinal and transverse cross sections in DVMP. In Fig. 10 we show the helicity correlations for $\pi^\pm$ photoproduction at $s = 10.3 \text{ GeV}^2$. They are very similar for these cases. In the backward hemisphere A_{LL} and K_{LL} are mirror symmetric which reflects the twist-3 dominance there. On the other hand, in the forward hemisphere where the twist-2 contribution becomes increasingly more significant A_{LL} and K_{LL} approach each other. The energy dependence of the helicity correlation parameters is very weak. π^0 photoproduction has been discussed by us in [16] in great detail. The helicity correlations for this channel reveal the approximate mirror symmetry in the forward hemisphere too since the twist-2 contribution is also tiny in that region; see Fig. 3.

As one sees from Eq. (50) there is only one independent nonvanishing twist-3 subprocess amplitude, namely $\mathcal{H}_{0-,-+}^{P,tw3}$ ($= -\mathcal{H}_{0+,+-}^{P,tw3}$ by parity conservation). This amplitude therefore cancels in (84) and, to twist-3 accuracy, the helicity correlations are solely expressed by the transversity form factors. In particular the numerator reads up to corrections of order κ

$$A_{LL}^{P,tw3} = -K_{LL}^{P,tw3} \propto -S_T^P \left(S_T^P - \frac{t}{2m^2} S_S^P \right). \tag{87}$$

Another spin-dependent observable is the correlation between the helicity of the incoming photon and the sideways polarization (i.e., the polarization perpendicular to the nucleon momentum but in the scattering plane) of the incoming (A_{LS}^P) or outgoing (K_{LS}^P) nucleon

$$A_{LS}^P = 2 \frac{\text{Re}[\Phi_{0+,++}^{P*} \Phi_{0-,-+}^P - \Phi_{0+,-+}^{P*} \Phi_{0-,++}^P]}{\sum_{\nu',\mu} |\Phi_{0\nu',\mu+}^P|^2},$$

$$K_{LS}^P = 2 \frac{\text{Re}[\Phi_{0+,++}^{P*} \Phi_{0-,++}^P - \Phi_{0+,-+}^{P*} \Phi_{0-,-+}^P]}{\sum_{\nu',\mu} |\Phi_{0\nu',\mu+}^P|^2}. \tag{88}$$

Predictions for these observables are displayed in Fig. 10 as well. Both twist 2 and twist 3 contribute substantially to
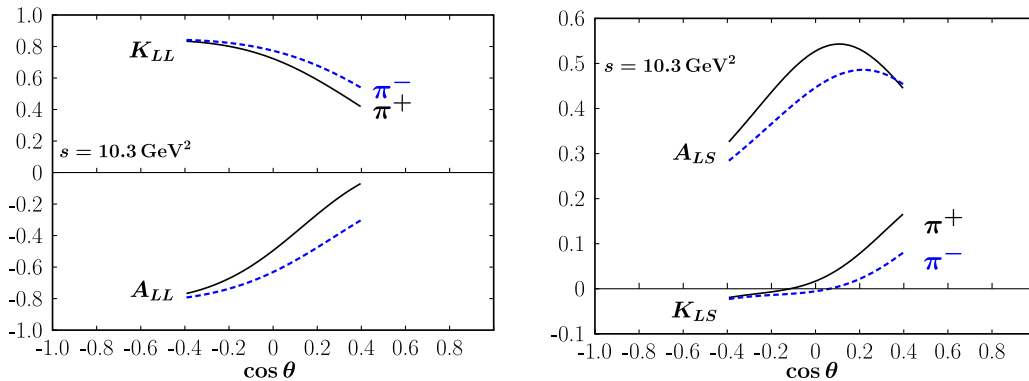

FIG. 10. Results for the helicity correlation parameters A_{LL}, K_{LL} (left) and A_{LS}, K_{LS} (right) for π^+ and π^- photoproduction vs $\cos\theta$ at $s = 10.3 \text{ GeV}^2$. Parameters as in [16].

these observables. The order $m/\sqrt{s}$ mass corrections (82) are also rather large for the LS correlations. In addition A_{LS} and K_{LS} are subject to strong cancellations among the contributions from various helicity amplitudes. In contrast to the helicity correlations, A_{LL} and K_{LL}, the mirror symmetry is therefore not to be seen for the LS correlations.

B. Helicity correlations in electroproduction

The helicity correlation A_{LL} can also be measured in pion electroproduction. In fact, the CLAS collaboration has measured it in the deeply virtual region [51]. In electroproduction there are two modulations of A_{LL}. Its $\cos(0\varphi)$ modulation, divided by $\sqrt{1-\varepsilon^2}$, is defined as in (84) except that the denominator is to be supplemented by the contribution from longitudinally polarized photons $\varepsilon(|\Phi_{0+,0+}|^2 + |\Phi_{0-,0+}|^2)$. The $Q^2 \to 0$ limit of $A_{LL}^{\cos(0\varphi)}/\sqrt{1-\varepsilon^2}$ is the A_{LL} parameter we discussed in the previous subsection. The second modulation of A_{LL} is related to the amplitudes by

$$\frac{A_{LL}^{P,\cos\varphi}}{\sqrt{\varepsilon(1-\varepsilon)}} \sigma_0^P = -\mathrm{Re}[(\Phi_{0+,++}^P + \Phi_{0+,-+}^P)\Phi_{0+,0+}^{P*}$$
$$+ (\Phi_{0-,++}^P + \Phi_{0-,-+}^P)\Phi_{0-,0+}^{P*}], \quad (89)$$

where

$$\sigma_0^P = \sum_{\nu',\mu}|\Phi_{0\nu',\mu+}^P|^2 + \varepsilon\sum_{\nu'}|\Phi_{0\nu',0+}^P|^2 \quad (90)$$

is the unseparated cross section without the phase space factor. We stress that for both the modulations of A_{LL} the longitudinal target polarization is defined relative to the direction of the virtual photon. In experiments the target polarization is usually defined relative to lepton beam direction. The transform from one definition to the other one is investigated in great detail in the work by Diehl and Sapeta [52]. According to that work, the following relation:

$$A_{LL}^{P,l} = \cos\theta_\gamma A_{LL}^P - \sin\theta_\gamma A_{LT}^P(\phi_S = 0) \quad (91)$$

holds for both the modulations. The angle ϕ_S denotes the orientation of the transversal target spin vector with respect to the lepton plane. The label l stands for the target polarization defined with respect to the lepton beam. The angle θ_γ describes the rotation in the lepton plane from the direction of the incoming lepton to that of the virtual photon. It is given by

$$\cos\theta_\gamma = \frac{1 + y\gamma^2/2}{\sqrt{1+\gamma^2}}, \quad (92)$$

where $\gamma = 2x_B m/Q$ and $y = (s + Q^2 - m^2)/(2mE_{Lab} + m^2)$ (x_B is Bjorken-x and E_{Lab} the beam energy in the Lab frame). Since this rotation requires information on the actual experiment which is not at our disposal, we refrain from quoting $A_{LL}^{P,l}$. The correlations $A_{LL}^{P,\cos(0\varphi)}/\sqrt{1-\varepsilon^2}$ and $A_{LL}^{P,\cos\varphi}/\sqrt{\varepsilon(1-\varepsilon)}$ still depend on ε through σ_0^P. In order to make predictions we have tentatively chosen $\varepsilon = 0.6$. The two modulations of A_{LL} are shown in Fig. 11 for π^+ electroproduction at $Q^2 = 1$ and 2 GeV^2 and $s = 10.3$ GeV^2. In order to facilitate the use of the possible transform (91) from the direction of the virtual photon to that of the lepton beam we also show in Fig. 11 the correlations between the lepton helicity and transversal target polarization defined by

$$\frac{A_{LT}^{P,\cos(0\varphi)}(\phi_s = 0)}{\sqrt{\varepsilon(1-\varepsilon)}} = -\frac{\mathrm{Re}[\Phi_{0+,++}^{P*}\Phi_{0-,0+}^P - \Phi_{0-,++}^{P*}\Phi_{0+,0+}^P]}{\sigma_0^P},$$
$$\frac{A_{LT}^{P,\cos\varphi}(\phi_s = 0)}{\sqrt{1-\varepsilon^2}} = -\frac{\mathrm{Re}[\Phi_{0+,++}^{P*}\Phi_{0-,-+}^P - \Phi_{0-,++}^{P*}\Phi_{0+,-+}^P]}{\sigma_0^P},$$
$$(93)$$

which also appear in (91).

A large variety of other spin-dependent observables exist for electroproduction of pions. Their study goes beyond the
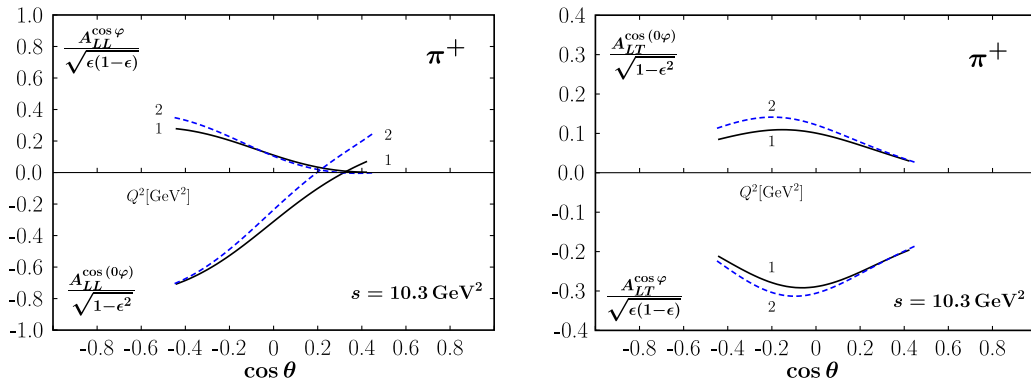

FIG. 11.   Results for the modulations of the helicity correlation A_{LL} (left) and the observable A_{LT} (right) for π^+ electroproduction vs $\cos\theta$ at $Q^2 = 1$ (solid) and 2 GeV^2 (dashed lines) at $s = 10.3$ GeV^2.

scope of the present work. Notice that the single-spin asymmetries frequently require phase differences. They are all zero for our LO study of the handbag mechanism, the LO amplitudes (9) and (11) are real.

VIII. REMARKS ON UNCERTAINTIES

There are two types of uncertainties. On the one hand, there are those resulting from the use of kinematics for which the prerequisite of the handbag approach namely that the Mandelstam variables should be much larger than a typical hadronic scale of order 1 GeV^2 is not sufficiently well respected. The analysis of the available photoproduction data as well as the photo- and electroproduction data to be expected in the near future force us to work in a kinematical situation in which the requirement of large Mandelstam variables is only marginally respected. On the other hand, there are the typical parametric uncertainties due to error-burdened parameters of the DAs and the form factors.

For Mandelstam variables which are not much larger than Λ^2 the problem arises how to match s, t and u for the hadronic process with the ones for the partonic subprocess, $\hat{s}, \hat{t}$ and $\hat{u}$. There are several possibilities to match the kinematics. They lead to different numerical results which may be regarded as different nucleon-mass corrections [53] of order m^2/s. Thus, one possibility is to identify the two sets of variables as in (8). Alternatively, one may use

$$\hat{t} = t, \qquad \hat{s} = s - m^2, \qquad \hat{u} = u - m^2, \qquad (94)$$

which choice guarantees the mass-shell condition for the subprocess, $\hat{s} + \hat{u} + \hat{t} = 0$. There are other possibilities [53]. For the kinematics of interest in this work the mass corrections due to the different matching recipes are large, in particular for $|\cos\theta| \to 1$. They amount to about 50% for photo- and electroproduction. However, for ratios of cross sections which we mainly present for electroproduction these mass corrections are smaller. Thus, for $d\sigma_T(Q^2)/d\sigma_T(0)$ and $d\sigma_{TT}(Q^2)/d\sigma_T(Q^2)$ they only amount to about 20% for not to large values of Q^2. For the helicity correlations, A_{LL} and K_{LL}, which likewise represent ratios of cross sections, the mass corrections are less than 20%.

The parametric uncertainty of the twist-3 contribution is very large. As mentioned in Sec. IV the parameters of the 3-body twist-3 DA have errors of about 30%. Together with the uncertainties of the large $-t$ behavior of the transversity form factors the parametric uncertainties of the cross sections amount to about 70% in the regions of twist-3 dominance. Evidently, for ratios of cross sections and for the helicity correlations the parametric uncertainties are much smaller since most of the uncertainties of the twist-3 DA cancel. The parametric uncertainty of the twist-2

contribution is insignificant compared to the other sources of errors.

IX. SUMMARY

We have calculated wide-angle photo- and electroproduction of pions within the handbag factorization scheme to twist-3 accuracy and LO of perturbative QCD. In this mechanism the amplitudes factorize into hard partonic subprocess amplitudes and soft form factors representing $1/x$-moments of zero-skewness GPDs. The twist-3 contributions to the subprocess amplitudes include the 2-body, $q\bar{q}$, as well as the 3-body, $q\bar{q}g$, Fock components of the pion. In light-cone gauge we are using for the vacuum-meson matrix elements, the equation of motion, which is formally an inhomogeneous linear first-order differential equation, fixes the 2-body twist-3 DAs, $\phi_{\pi p}$ and $\phi_{\pi\sigma}$, for a given 3-body DA. Thus, only two independent pion DAs remain as soft physics input to the handbag mechanism in addition to the form factors, the usual ones, being related to the helicity nonflip GPDs, as well as the transversity form factors. Taking the DAs and the form factors from our previous work [16], we evaluated the photoproduction cross sections within the handbag mechanism and compared the results with experimental data. It seems that the energy dependence of the handbag contribution is somewhat too strong. Including evolution and the t-dependence of the form factors it is approximately s^{-9} at fixed $\cos\theta$. Therefore, as an alternative we also presented results evaluated at the fixed scale of 1 GeV which agree fairly well with experiment. A better determination of the large $-t$ behavior of the form factors is required before a final answer can be given what the energy dependence of handbag predictions is. We also give detailed predictions for pion electroproduction and discuss spin effects, especially helicity correlations. The gross features of wide-angle electroproduction bear similarities to DVMP: the π^0 channel is dominated by the twist-3 contributions, for the $\pi^\pm$ channels twist-2 contributions matter in the forward hemisphere. Data on pion electroproduction would allow to extract detailed information on the large $-t$-behavior of the form factors and the transversity GPDs at zero skewness. This knowledge bears implications of our understanding of the parton densities in the transverse position plane [54,55]. It may also be of help in understanding some of the spin density matrix elements of deeply virtual vector-meson production [56,57]. In the present work, we restricted ourselves to the case of the pion. However, the generalization to other pseudoscalar mesons is straightforward.

ACKNOWLEDGMENTS

APPENDIX: THE EVOLUTION OF THE PION DAs

In this Appendix we compile the anomalous dimensions needed to evolve the DAs used in the previous sections. The anomalous dimensions can be found in [29,31]. The evolution goes with the quantity

$$L = \frac{\alpha_S(\mu_R)}{\alpha_S(\mu_O)} = \frac{\ln(\mu_0^2/\Lambda_{\text{QCD}}^2)}{\ln(\mu_R^2/\Lambda_{\text{QCD}}^2)}. \quad \text{(A1)}$$

The second Gegenbauer coefficient of the twist-2 pion DA evolves as

$$a_2(\mu_R) = a_2(\mu_0)L^{\gamma_2/\beta_0}, \quad \text{(A2)}$$

with $\gamma_2 = 50/9$ and $\beta_0 = (11N_C - 2n_f)/3$. The mass parameter, μ_π evolves as

$$\mu_\pi(\mu_R) = L^{-4/\beta_0}\mu_\pi(\mu_0). \quad \text{(A3)}$$

The parameters of the 3-body DA evolve as

$$f_{3\pi}(\mu_F) = L^{(16/3C_F-1)/\beta_0}f_{3\pi}(\mu_0),$$

$$\omega_{1,0}(\mu_R) = L^{(-25/6C_F+11/3C_A)/\beta_0}\omega_{1,0}(\mu_0),$$

$$\omega_{11}(\mu_R) = \frac{1}{\gamma_+ - \gamma_-}[(\gamma_- - \gamma_{11})A_+(\mu_0)L^{(\gamma_+-16/3C_F+1)/\beta_0} + (\gamma_+ - \gamma_{11})A_-(\mu_0)L^{(\gamma_--16/3C_F+1)/\beta_0}],$$

$$\omega_{20}(\mu_R) = \frac{1}{4}\frac{\gamma_{21}}{\gamma_- - \gamma_+}[A_+(\mu_0)L^{(\gamma_+-16/3C_F+1)/\beta_0} + A_-(\mu_0)L^{(\gamma_--16/3C_F+1)/\beta_0}], \quad \text{(A4)}$$

where

$$A_+(\mu_0) = -\omega_{11}(\mu_0) - 4\frac{\gamma_+ - \gamma_{11}}{\gamma_{21}}\omega_{20}(\mu_0),$$

$$A_-(\mu_0) = \omega_{11}(\mu_0) + 4\frac{\gamma_- - \gamma_{11}}{\gamma_{21}}\omega_{20}(\mu_0). \quad \text{(A5)}$$

The anomalous dimensions are

$$\gamma_{11} = \frac{122}{9}, \quad \gamma_{22} = \frac{511}{45}, \quad \gamma_{12} = \frac{5}{3}, \quad \gamma_{21} = \frac{21}{5}, \quad \text{(A6)}$$

with the eigenvalues

$$\gamma_\pm = \frac{1}{2}\left[\gamma_{11} + \gamma_{22} \pm \sqrt{(\gamma_{11} - \gamma_{22})^2 + 4\gamma_{12}\gamma_{21}}\right]. \quad \text{(A7)}$$

[1] X. D. Ji, Phys. Rev. D **55**, 7114 (1997).

[2] J. C. Collins, L. Frankfurt, and M. Strikman, Phys. Rev. D **56**, 2982 (1997).

[3] A. V. Radyushkin, Phys. Rev. D **58**, 114008 (1998).

[4] M. Diehl, T. Feldmann, R. Jakob, and P. Kroll, Eur. Phys. J. C **8**, 409 (1999).

[5] M. Diehl, T. Feldmann, R. Jakob, and P. Kroll, Eur. Phys. J. C **39**, 1 (2005).

[6] M. Diehl and P. Kroll, Eur. Phys. J. C **73**, 2397 (2013).

[7] A. Danagoulian et al. (Hall A Collaboration), Phys. Rev. Lett. **98**, 152001 (2007).

[8] H. W. Huang and P. Kroll, Eur. Phys. J. C **17**, 423 (2000),

[9] H. W. Huang, R. Jakob, P. Kroll, and K. Passek-Kumerički, Eur. Phys. J. C **33**, 91 (2004).

[10] S. V. Goloskokov and P. Kroll, Eur. Phys. J. C **65**, 137 (2010).

[11] S. V. Goloskokov and P. Kroll, Eur. Phys. J. A **47**, 112 (2011).

[12] A. Airapetian et al. (HERMES Collaboration), Phys. Lett. B **682**, 345 (2010).

[13] I. Bedlinskiy et al. (CLAS Collaboration), Phys. Rev. Lett. **109**, 112001 (2012).

[14] M. Defurne et al. (Jefferson Lab Hall A Collaboration), Phys. Rev. Lett. **117**, 262001 (2016).

[15] M. C. Kunkel et al. (CLAS Collaboration), Phys. Rev. C **98**, 015207 (2018).

[16] P. Kroll and K. Passek-Kumerički, Phys. Rev. D **97**, 074023 (2018).

[17] A. V. Belitsky, A. Kirchner, D. Mueller, and A. Schafer, Phys. Lett. B **510**, 117 (2001).

[18] G. P. Lepage and S. J. Brodsky, Phys. Rev. D **22**, 2157 (1980).

[19] A. V. Efremov and A. V. Radyushkin, Phys. Lett. **94B**, 245 (1980).

[20] G. R. Farrar, K. Huleihel, and H. y. Zhang, Nucl. Phys. **B349**, 655 (1991).

[21] R. L. Anderson, D. Gustavson, D. Ritson, G. A. Weitsch, H. J. Halpern, R. Prepost, D. H. Tompkins, and D. E. Wiser, Phys. Rev. D **14**, 679 (1976).

[22] T. C. Brooks and L. J. Dixon, Phys. Rev. D **62**, 114021 (2000).

[23] M. Vanderhaeghen, P. A. M. Guichon, and J. Van de Wiele, Nucl. Phys. **A622**, c144 (1997).

[24] I. V. Anikin and O. V. Teryaev, Phys. Lett. B **554**, 51 (2003).

[25] I. V. Anikin, D. Y. Ivanov, B. Pire, L. Szymanowski, and S. Wallon, Nucl. Phys. **B828**, 1 (2010).

[26] M. Beneke and T. Feldmann, Nucl. Phys. **B592**, 3 (2001).

[27] P. A. Zyla et al. (Particle Data Group), Prog. Theor. Exp. Phys. **2020**, 083C01 (2020).

[28] T. Huang, X. H. Wu, and M. Z. Zhou, Phys. Rev. D **70**, 014013 (2004).

[29] P. Ball, J. High Energy Phys. 01 (1999) 010.

[30] J. B. Kogut and D. E. Soper, Phys. Rev. D **1**, 2901 (1970).

[31] V. M. Braun and I. E. Filyanov, Z. Phys. C **48**, 239 (1990); Yad. Fiz. **52**, 199 (1990) [Sov. J. Nucl. Phys. **52**, 126 (1990)].

[32] H. C. Lee and M. S. Milgram, Phys. Rev. Lett. **55**, 2122 (1985).

[33] P. V. Landshoff, Phys. Lett. **169B**, 69 (1986).

[34] X. D. Ji, J. Phys. G **24**, 1181 (1998).

[35] P. Kroll, K. Passek-Kumerički, and L. Szymanowski (to be published).

[36] V. M. Braun, S. Collins, M. Gckeler, P. Prez-Rubio, A. Schäfer, R. W. Schiel, and A. Sternbeck, Phys. Rev. D **92**, 014504 (2015).

[37] L. L. Frankfurt, P. V. Pobylitsa, M. V. Polyakov, and M. Strikman, Phys. Rev. D **60**, 014010 (1999).

[38] G. F. de Teramond, T. Liu, R. S. Sufian, H. G. Dosch, S. J. Brodsky, and A. Deur (HLFHS Collaboration), Phys. Rev. Lett. **120**, 182001 (2018).

[39] H. Moutarde, P. Sznajder, and J. Wagner, Eur. Phys. J. C **78**, 890 (2018).

[40] S. Alekhin, J. Blümlein, and S. Moch, Phys. Rev. D **86**, 054009 (2012).

[41] P. Kroll, Eur. Phys. J. A **53**, 130 (2017).

[42] D. J. Hamilton et al. (Jefferson Lab Hall A Collaboration Collaboration), Phys. Rev. Lett. **94**, 242001 (2005).

[43] C. Fanelli et al., Phys. Rev. Lett. **115**, 152001 (2015).

[44] S. D. Drell and T. M. Yan, Phys. Rev. Lett. **24**, 181 (1970).

[45] S. J. Brodsky, M. Burkardt, and I. Schmidt, Nucl. Phys. **B441**, 197 (1995).

[46] F. Yuan, Phys. Rev. D **69**, 051501 (2004).

[47] L. Y. Zhu et al. (Jefferson Lab Hall A and Jefferson Lab E94-104 Collaboration), Phys. Rev. C **71**, 044603 (2005).

[48] M. Diehl, Eur. Phys. J. C **19**, 485 (2001).

[49] A. Krassnigg and H. C. Pauli, Nucl. Phys. B, Proc. Suppl. **108**, 251 (2002).

[50] H. W. Huang, P. Kroll, and T. Morii, Eur. Phys. J. C **23**, 301 (2002); **31**, 279(E) (2003).

[51] A. Kim, H. Avakian, V. Burkert, K. Joo, W. Kim, K. P. Adhikari, Z. Akbar, S. Anefalos Pereira, R. A. Badui, M. Battaglieri et al., Phys. Lett. B **768**, 168 (2017).

[52] M. Diehl and S. Sapeta, Eur. Phys. J. C **41**, 515 (2005).

[53] M. Diehl, T. Feldmann, H. W. Huang, and P. Kroll, Phys. Rev. D **67**, 037502 (2003).

[54] M. Burkardt, Int. J. Mod. Phys. A **18**, 173 (2003).

[55] M. Diehl and P. Hagler, Eur. Phys. J. C **44**, 87 (2005).

[56] S. V. Goloskokov and P. Kroll, Eur. Phys. J. C **53**, 367 (2008).

[57] S. V. Goloskokov and P. Kroll, Eur. Phys. J. C **74**, 2725 (2014).